

Review

A Review of Orbital Friction Stir Welding

Francisco B. Ferreira ¹, Igor Felice ¹ , Isaque Brito ¹ , João Pedro Oliveira ²  and Telmo Santos ^{1,3,*} 

¹ UNIDEMI, Department of Mechanical and Industrial Engineering, School of Science and Technology, NOVA University Lisbon, 2829-516 Caparica, Portugal

² CENIMAT | i3N, Department of Materials Science, School of Science and Technology, NOVA University Lisbon, 2829-516 Caparica, Portugal

³ Laboratório Associado de Sistemas Inteligentes, LASI, 4800-058 Guimarães, Portugal

* Correspondence: telmo.santos@fct.unl.pt

Abstract: Friction stir welding is a solid-state joining process widely used in several industrial applications. One of its variants, orbital friction stir welding, is of key importance in fundamental industries such as oil and gas and aerospace. For orbital friction stir welding, there is a need to develop not only new process parameters but also tools and ancillary mechanisms that can ensure sound, high-performing joints are obtained. This review assesses the current state of orbital friction stir welding, highlighting several key aspects related to this technology.

Keywords: friction stir welding; orbital friction stir welding; mechanical properties; microstructure

1. Introduction

The literature dedicated to orbital friction stir welding (OFSW) is scarce nowadays, despite the huge technological potential of this solid-state welding process. In this sense, this work aims to provide a summary and synthesis of the current knowledge pertaining to this topic while also pinpointing areas that require further investigation by identifying gaps, trends, and patterns. This review holds the potential to serve as a useful tool for researchers, offering valuable insights, particularly for those interested in OFSW. The process is based on conventional friction stir welding (FSW), depicted in Figure 1, and was initially patented by TWI [1] in 1991. Then, in 2001, Ding et al. patented an orbital friction stir weld system [2]. Since then, several developments have been performed, and in 2016, Peterson et al. patented a system for OFSW for small-diameter tubing or pipes [3]. Conventional FSW employs a non-consumable tool with linear motion to join two metal plates through the application of frictional heat, causing the material to soften and become viscous, ultimately resulting in a solidified welding bead. Conversely, OFSW utilizes a tool with an orbital motion in addition to its linear motion, allowing for the generation of a circular weld path and the creation of full-circle welds. This method is particularly useful for joining complex geometries due to its improved flexibility and control, thus increasing the industrial applicability of the process [1–3]. Rams et al., for example, applied this method to welding hemispheres of cast aluminum alloy for valves [4].



Citation: Ferreira, F.B.; Felice, I.; Brito, I.; Oliveira, J.P.; Santos, T. A Review of Orbital Friction Stir Welding. *Metals* **2023**, *13*, 1055. <https://doi.org/10.3390/met13061055>

Academic Editor: Huihuan Ma

Received: 13 February 2023

Revised: 17 May 2023

Accepted: 22 May 2023

Published: 31 May 2023



Copyright: © 2023 by the authors. Licensee MDPI, Basel, Switzerland. This article is an open access article distributed under the terms and conditions of the Creative Commons Attribution (CC BY) license (<https://creativecommons.org/licenses/by/4.0/>).

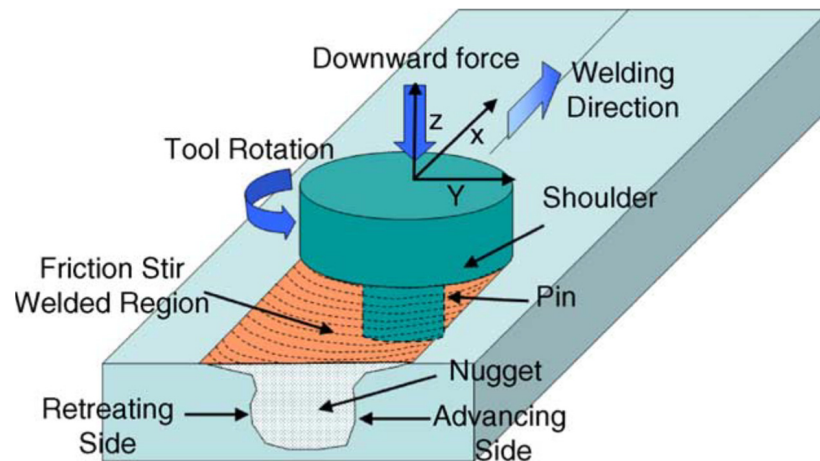


Figure 1. Conventional FSW process and main nomenclatures, reprinted with permission from [5], 2023, Elsevier.

2. Advantages and Limitations of FSW over Fusion Welding

The concept of generic orbital welding dates back to the early 1960s, when it was developed to provide better conditions for the manufacture of components for the aerospace industry. The first dedicated orbital welding apparatus was developed and patented by Rohrberg et al. in 1966 [6]. A representative orbital GTA welding system is illustrated in Figure 2. Nowadays, several orbital welding systems are commercially available. However, in aerospace applications, as a consequence of flight speeds close to the speed of sound, by exposing these welding joints to extreme vibrations and mechanical stresses, failures of those joints tended to appear and rapidly became a problem that demanded a more viable joining technology [7].

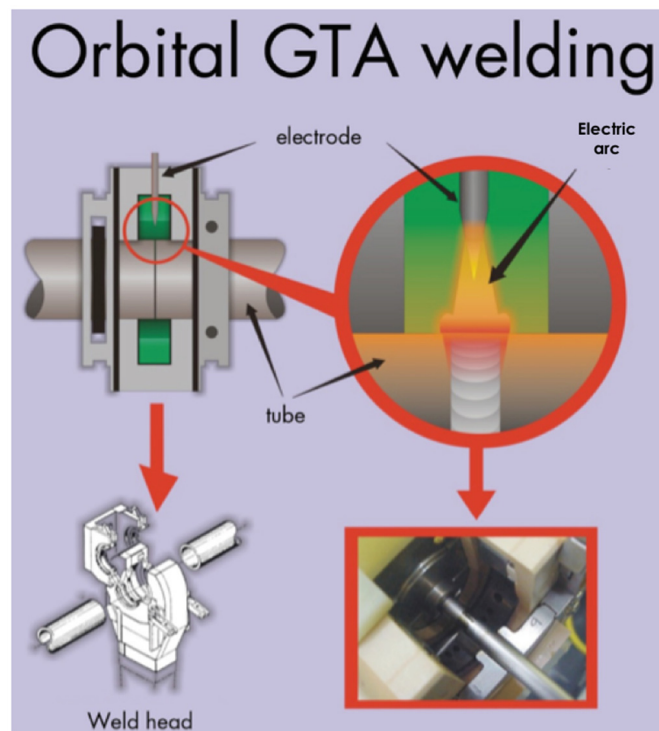


Figure 2. Representative illustration of orbital GTA welding, reprinted with permission from [7], 2023, Departamento de Ciencia e Tecnologia Aeroespacial.

Even though this review is about FSW and in particular its orbital variant, it seems appropriate and useful to compare this technology with conventional fusion welding methods since both technologies have their applications and studies are still being conducted to improve them. Therefore, this chapter focuses on the comparison between technologies, highlighting their advantages and limitations.

The solid-state nature of the FSW process is what immediately distinguishes it from the conventional welding techniques widely adopted in diverse industries, such as aerospace, automotive, oil and gas, and others. There is a broad diversity of fusion welding technologies, such as shielded metal arc welding (SMAW), gas metal arc welding (GMAW), gas tungsten arc welding (GTAW), and electron beam and laser welding, and the heat source type is the main differentiating aspect [8].

Since there is neither fusion nor the addition of filler material in the FSW, it is possible to join a wider range of materials compared to conventional fusion welding due to the fact that the composition compatibility of the materials to be joined is not a process requirement, unlike conventional fusion welding [5]. Given that, it is possible to effectively join dissimilar materials as well as specific materials that are difficult to weld using conventional methods, such as high-strength aluminum alloys, due to their high conductivity and reflectivity [9]. Finally, the molten pool's dynamic behavior during fusion welding is a challenging phenomenon, and it is currently the focus of several investigations that, primarily using theoretical-computational simulations, seek to characterize the dynamics, control instability, and predict common solidification defects. FSW/OFSW has been shown to mitigate most of these concerns [10,11].

The FSW process evades typical defects resulting from the material's solidification, including porosities, cracks, and oxygen contamination, due to the absence of fusion. Yet, the process is not free from defects such as flashes, voids, wormholes, and joint line remnants if the parameters are inappropriate for the given application. Indeed, welding parameters, such as rotational speed, travel speed, axial force, plunge depth, and tool selection, should be thoroughly monitored and controlled; however, those parameters are commonly selected prior to the process and maintained along the weld path, benefiting from an automated and repeatable process. Although automated orbital fusion systems have been developed [12], the success of the weld depends upon a wider range of parameters when compared to FSW, and some are extremely arduous to monitor and control, such as variations in the power supply and wire chemical composition that may jeopardize the integrity of the weld [13]. For instance, despite the excellent quality and control, material range, and clean work environment (minimal spatter and fumes), achieving a successful weld by orbital GTAW technology highly depends on a series of boundary conditions, such as the chemical composition of the material, setup requirements, type and purity of the gases, and type and geometry of the electrodes, in addition to the primary welding parameters, namely the heat input (which is dependent on current, arc voltage, and travel speed), wire extension or "stick-out", wire diameter, and torch angle. The use of shielding gas is intrinsically related to fusion welding technologies [13] and is not mandatory in FSW for the majority of metals. Additionally, GTA welds, when compared to FSW, are more susceptible to distortion, have a lower welding speed, and can be more affected by impurities, leading to defects and porosity in the weld. The exception includes some high-temperature alloys, such as titanium alloys, due to their intense reactivity that leads to material contamination by atmospheric nitrogen, oxygen, and hydrogen, and ceramic and refractory tools that require protection from oxidation. Using the shielding gas in these cases, typically argon, is not mandatory but highly recommended, not only to guarantee the integrity and quality of the weld but also to extend the tool's life [5].

It is generally accepted that FSW is a cleaner and safer technology than conventional welding methods since fumes, electric arcs, molten spatters (in GMAW and PAW), or radiation hazards are not associated with this solid-state process. The emission of nanoparticles and microparticles during the processing of aluminum alloys has been demonstrated [14], despite the fact that their biological and toxic consequences are yet to be determined. Thus,

concerning the environmental benefits, FSW is clearly a better alternative. Firstly, no special pre-weld profiling or surface cleaning is required, in contrast to fusion methods [13], eliminating grinding waste and solvents for degreasing prior to the welding process. Then, during the process for the majority of materials, there are no typical welding consumables, such as filler material and gases [5]. In addition to that, FSW is not only a high-efficiency process (required heating takes place at the tool/workpiece interface), but the energy consumption is also much lower than in fusion methods, being mostly related to driving the welding spindle. Previous studies reported that FSW can be conducted with only 2.5% of the energy needed for laser welding [5]. Considering that, particularly for the industry where high productivity and profit are two targets, FSW and OFSW can be very appealing despite the higher initial investment in equipment and tools. As previously stated, no consumables are required to perform FSW except the tool, which has limited usage. Joining low-temperature materials, such as aluminum or magnesium alloys, can be easily achieved with the use of steel tools, while for high-temperature alloys, such as titanium, ceramic and refractory tools are a better choice. A review of the types, materials, shapes, and features of FSW tools is presented in the next chapter of this work. Another indirect way to compare costs between technologies is to evaluate the time required to successfully produce good welds, and FSW can be much more time-efficient for numerous reasons, not only prior to the process due to the few requirements of workpiece preparation but also during the process and after it. Engelhard et al. [15] revealed that, in addition to the better mechanical properties achieved through OFSW of AA5754, AA5083, and AA6106 alloys, the welding time was 40% shorter than that of orbital TIG welds. The capability of full penetration in a single pass, i.e., being able to perform single-pass welds without stopping, results in a shorter processing time as well as a lower susceptibility to welding failures. Although higher welding speeds (up to 8 mm/s) [16] have been reported in orbital GTAW when compared to FSW, the need for several filling passes makes the overall process slower. In this study, despite the reported defect-free welds of AISI 304 L stainless steel in pipes for the abovementioned travel speeds, no mechanical characterization was conducted. Other time- and cost-saving attributes of FSW and OFSW are associated with the minimum post-welding processes required, such as low degrees of distortion leading to greater assembly precision and, consequently, reduced need for rectification, a lack of spatters to be removed, and a smooth welding surface with little to no flash if the optimal parameters are adopted. However, attention is required as a slight mismatch can compromise the results, leading to excessive flash, as the process is sensitive to joint tolerances. Furthermore, due to the solid-state nature and high repeatability of FSW, minimal post-weld inspection is necessary [17]. A lack of full penetration, as a consequence of the commonly used fixed pin/probe length tools, might result in “kissing bond” defects that are typically difficult to detect by non-destructive testing [18].

As FSW/OFSW and conventional fusion processes have their differences, the metallographic properties of the welds are no exception, with distinctive microstructural and mechanical properties. As it is a solid-phase process and consequently is able to join materials at lower temperatures than conventional fusion methods, several metallurgical benefits can be identified, such as little to no distortion and/or shrinkage of the workpiece, which promotes good dimensional stability and high repeatability of the process. The mechanical properties of the welded material are commonly referred to as far superior in FSW/OFSW, particularly in strengthened aluminum alloys, which usually have a 20% increase in as-welded ultimate tensile strength relative to fusion welding [18], as dissolution of alloying elements is typically avoided [5]. In addition, the lower temperature results in less harm in the welded heat-affected zone [18]. Indeed, these benefits tend to be consistent for the majority of low-temperature alloys, especially those submitted to age or solution heat treatments; however, when joining high-temperature alloys, the supremacy of the metallurgical properties in FSW/OFSW is not so indisputable, as high joining efficiencies up to 91.5% have been demonstrated when welding small-diameter tubes of grade 2 pure titanium [7] using GTAW technology. The “stirring” effect characteristic of FSW is able to

generate a dynamically recrystallized stir zone with an extremely fine grain structure that may have a positive influence on mechanical properties at room temperature. For instance, hardness, yield strength, ultimate tensile strength, impact strength, and fatigue properties are dependent on the grain size and tend to increase as the grain size decreases [19].

Although for distinct reasons, a common concern when performing orbital welding not only by OFSW but also by fusion technologies is the “start-end” point. Despite the fact that no major defects were visually identified by dye penetrant inspection for most of the dissimilar material welding (SS304 and BS1387), Ayof et al. [8] reported consistently unsatisfactory results at the start-end point due to a lack of fusion. In contrast, the start and stop overlap in OFSW should be of higher quality, as the process performs better when welded on itself. However, the preeminent concern at the end of an OFSW procedure is the hole left in the workpiece resulting from the pin/probe tool extraction, typically referred to as a “keyhole.” Although the keyhole can compromise the integrity of the weld, several solutions or equipment adaptations can be adopted in order to avoid this issue. Some of them will be further discussed in this work, and a general table with a summary of the main advantages of FSW/OFSW over fusion welding is presented in Table 1.

Table 1. Summary of the main advantages of FSW/OFSW over fusion welding.

Advantages of FSW/OFSW over Fusion Welding
No filler or material addition is required
No fusion process is involved
Applicable to a wider range of materials
Dissimilar materials can be joined effectively
Evades typical solidification defects
Easier to automate
Higher repeatability (good dimensional stability)
Fewer boundary conditions (parameters) are needed
Cleaner and safer technology
Higher efficiency and lower energy consumption
Little to no workpiece distortion and/or shrinkage
Mechanical properties are referred to as superior

3. Process and Variants

3.1. FSW Tools

Choosing a suitable tool for any FSW application is crucial in the pursuit of a perfect weld; therefore, it must not be neglected. Since extensive and valuable reviews of FSW tools have already been published [5,20,21], this chapter focuses on a brief description of the most frequently used tools in FSW applications, with particular emphasis on tool shapes and features more suitable for OFSW experiments, given their high popularity among published works.

Generally, and simplifying, a tool of FSW is composed of a shoulder and a pin/probe. The shoulder is responsible for most of the friction heat, making forging action mandatory for welding consolidation and material containment, whereas the pin/probe’s main responsibility is “stirring,” i.e., plastic deformation and material flow. Note that this is not so trivial given that, depending on tool features and shapes, the shoulder can have an influence on material flow and the probe can contribute to the generation of heat. FSW tools can be categorized into three types, namely, fixed, adjustable, and self-reacting, and are presented in Figures 3–5.

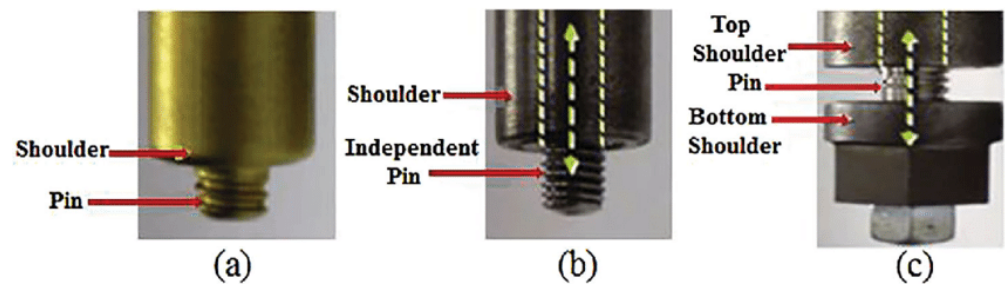


Figure 3. Examples of FSW tools: (a) fixed; (b) adjustable; (c) self-reacting, reprinted with permission from [21], 2023, Taylor & Francis.

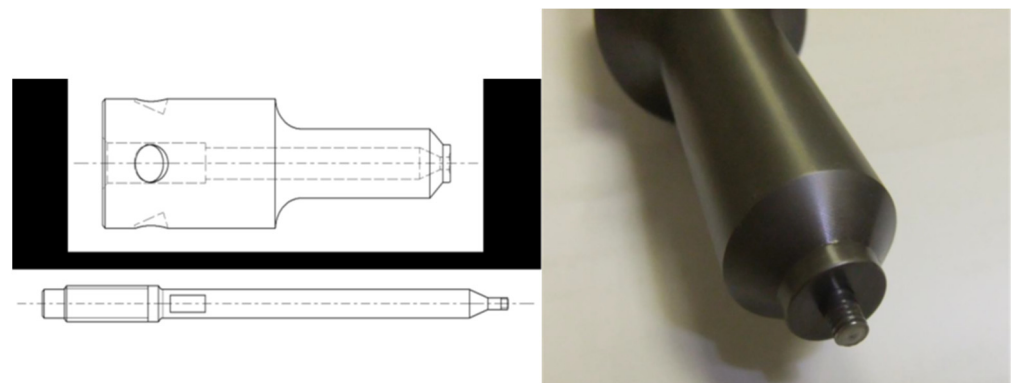


Figure 4. Adjustable-type pin tool, reprinted with permission from [22], 2023, Elsevier.

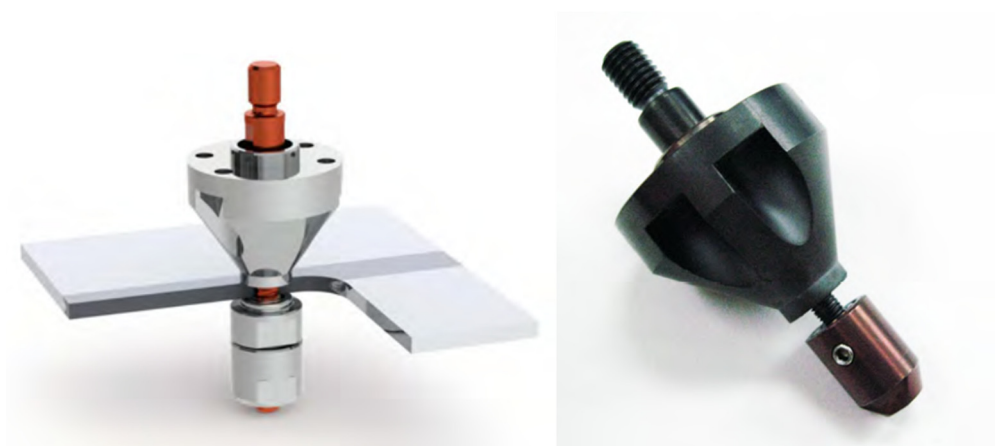


Figure 5. Bobbin-type tool, reprinted with permission from [23], 2023, Taylor & Francis.

The fixed probe tool, depicted in Figure 3a, is the simplest and most common type of tool in FSW, and since it is composed of a single piece, it tends to be the cheapest tool. However, it has some drawbacks and limitations, especially when joining structures with thickness deviations, due to the limited fixed pin length. Furthermore, adopting the fixed probe tool in FSW/OFSW requires a back anvil to support the applied axial force characteristic of the process in order to avoid workpiece collapse, and if the probe becomes damaged or worn out, the whole tool must be replaced. However, this type of tool allows for the implementation of the process with a tilt angle, which improves the material flow behind the FSW tool and prevents defects from forming [24].

Despite the higher cost, the adjustable tools (Figures 3b and 4) can be more advantageous than fixed tools in some applications, considering that they are composed of at least two individual pieces that can be built from different materials and, if one damages or wears out, it can be easily replaced. As the name of the tool suggests, the pin/probe

length can be adjusted to suit the requirements of the material to be joined or processed. Some tools can even be adjusted during the process, such as the retractable pin patented by NASA [25], which can be very beneficial if the thickness of the specimens is not constant along the path. The retractable pin can also be used as a mechanism to avoid the inevitable defect created during the extraction of the tool at the end of the process, referred to as a keyhole, which may not be acceptable for most orbital welding applications. Nonetheless, there are other approaches to preventing the keyhole defect, such as using a run-off ramp [26], which will be better explained later in this work. Similar to the fixed probe tools, the adjustable ones also require a back anvil and allow the use of a tilt angle during the process.

Finally, the remaining tool type is the self-reacting or bobbin one, depicted in Figures 3c and 5, which tends to be the least common despite its apparent advantages over the others. Composed mainly of three separated pieces: the top shoulder, the pin/probe, and the bottom shoulder, the self-reacting tool stands out not only because the pin/probe length can be adjusted similar to the adjustable tool but also because it does not depend on a backing anvil. On the other hand, this type of tool can only work perpendicularly to the surface of the workpiece, so it will not be possible to benefit from the use of a tilt angle.

In summary, and focusing on the orbital variant of FSW, all the described tools are suitable to carry out the process, with varying advantages and limitations. One of the major issues in OFSW is the presence of a keyhole defect at the end of the process, so at first glance, adjustable tools, such as the retractable pin, seem to be the simpler and easier choice; however, identical results can be achieved using a low-cost, fixed probe tool if some modifications are made to the OFSW equipment or apparatus. The other major limitation of OFSW is the requirement of a backing anvil to support the workpiece throughout the process. As will be referred to later, internal mandrels are typically used in order to avoid the collapse of the specimens, consequently increasing the complexity of the equipment or apparatus needed to perform OFSW. Therefore, the self-react tool is also a viable option for joining cylindrical workpieces such as tubes or pipes. However, if a sealed container, such as an aerospace fuel tank, needs to be welded, both the self-react and bobbin tools, assisted by the inner mandrel, are not viable on their own because the interior of the “container” becomes inaccessible to remove the bottom shoulder or the inner mandrel, respectively, and adaptations should be made to the workpiece.

3.1.1. Tool Materials

The tool material is one more aspect that greatly influences the process as it can affect the quality of the weld since its properties, such as strength, fracture toughness, hardness, thermal conductivity, and thermal expansion coefficient, may impact the generation and dissipation of heat, performance, and tool wear [20,21]. Since there are no specific and conclusive studies about OFSW applications, it is assumed that the selection of the tool's material follows the same criteria as linear FSW, thus being mainly dependent on the workpiece material and desired tool life. When deciding the tool material for a given application, not only the weld quality must be considered but also its wear and reusability, which are of major importance due to the impact they can have on the process's cost efficiency. As already mentioned, the tool material's properties are of great importance to the process. Ideally, an FSW tool should have good machinability to facilitate the implementation of complex shoulder and pin/probe features, an affordable cost, avoid adverse reactions (such as oxidation), good strength, creep resistance, and dimensional stability. Additionally, the tool should have good fracture toughness to avoid harm from plunging and dwelling. Due to the forging forces applied to the tool during the process, it must have a high compressive yield strength at high temperatures in order to withstand the applied loads. The reusability of the tool implies numerous heating and cooling cycles, and thus having good thermal fatigue strength is required to extend the tool's life. Particularly in tools where the pin/probe and the shoulder are composed of different materials, the coefficient of thermal

expansion of the two should be similar to diminish the thermal stresses, something that can be achieved by using a thermal barrier coating [21]. Unfortunately, currently, there is not a tool material that matches perfectly with the abovementioned criteria to be generally applied in welding of all types of material.

To simplify, the tool materials can be placed into two categories depending on the materials to be joined, i.e., soft alloys, such as aluminum and magnesium, and high-strength alloys, such as steel and titanium.

When joining soft alloys, there is consensus on adopting tool steels, such as AISI H13, because their properties can accurately match most of the ideal criteria previously stated. It has been demonstrated to be perfectly adequate for welding aluminum alloys with thicknesses from 0.5 mm up to 50 mm [27], as well as welding distances up to 5 km [28], in addition to its affordable cost and good machinability. However, in high-strength alloy applications, such long-life and affordable tools are not currently available, and some compromises should be established. Despite the variety of materials capable of performing FSW/OFSW in these alloys, none is without setbacks. Currently, polycrystalline cubic boron nitride (PCBN) tools are highly popular and are able to perform good-quality welds due to their high strength, hardness, and stability when subjected to high temperatures, allowing these tools to wear at slower rates than other tools. However, PCBN tools also exhibit poor machinability and low fracture toughness, which can hamper the manufacture of more complex geometries and tool features. In addition to that, the high pressure and high temperature processes that sintering cubic boron nitride requires, as well as its limited size, make these tools relatively expensive. Refractory metals, such as tungsten, molybdenum, niobium, and tantalum, can also be used as tool materials since most of these alloys are produced as single-phase materials and their mechanical properties are preserved up to 1000–1500 °C, granting them wonderful high-temperature strength. However, and similarly to the PCBN tools, these alloys have a relatively high cost as their primary production technology is powder processing. Other possible options for tool materials that offer high strengths, ductility, good creep, and corrosion resistance are nickel- and cobalt-based superalloys. Since these superalloys have low machinability, they are suitable for simpler designs, which prevents them from manufacturing more complex tool features, such as flutes and flats. There have been attempts to use ceramic particle-reinforced metal matrix composites (MMCs) as tool materials, but due to their brittle nature, fractures might occur during the tool plunging phase of the process. Frequently used as machining tools, some carbide materials can also be viable alternatives to perform FSW/OFSW at ambient temperature, benefiting from admirable wear resistance as well as acceptable fracture toughness. One more promising tool material, despite not being ordinarily used yet, is silicon nitride (Si_3N_4), which has already been able to produce quality welds comparable to PCBN tools at a significantly lower cost.

To summarize, almost 30 years after the invention of FSW, several innovations in the tool material category have already been established. Particularly in welding and/or processing the softer alloys, the available tool materials already have exceptional long lives for a reasonable acquisition price. Despite still having room for improvement, further developments and innovations for these tools are more likely to target tool design features, as they can have a tremendous impact on the process, with the intention of making FSW/OFSW as efficient as possible. On the other hand, even with the variety of already available tool materials to perform FSW/OFSW on high-strength alloys, further advancements are needed to address the existing issues regarding excessive tool cost and limited tool life.

3.1.2. Tool Dimensions

The success of an FSW/OFSW procedure relies upon the capability of generating enough heat to allow the flow of the plasticized material and consequently create the weld joint. The FSW forces and heat input are not only greatly influenced by parameters such as tool rotation speed, welding speed, pressure, shear stress, and friction coefficient, but also by the geometric parameters of the tool that directly impact the forces and heat

input [5,20,21,29,30]. A framework of the relation between the process parameters and their influence on the process forces, heat generation, and occurrence of defects will be discussed later in this work, whereas in this subchapter, emphasis will be given to the tool dimensions, namely the pin length, pin diameter, and shoulder diameter. When choosing a pin/probe length for a given application, not only should the workpiece thickness be accounted for but also the tool tilt (if applicable) and the desired clearance between the end of the pin and the backing anvil. Regarding its diameter, a trade-off should be settled since a larger pin diameter is more likely to resist the transverse loads during the process, hence avoiding its fracture; however, a smaller pin diameter enhances the workpiece material consolidation behind the tool before cooling [5]. Tufaro et al. [31] studied the effect that the shoulder diameter has on heat generation, concluding that it is associated with different characteristics of the welded joints. The authors reported that when adopting a smaller tool shoulder diameter, defects located at the base of the welding nugget tended to occur due to a lack of plastic flow. In contrast, when a larger shoulder diameter was used, not only a steeper decrease in the nugget hardness was observed as a consequence of a grain size increase but also an enlargement of that hardness-affected zone, indicating that increasing the shoulder diameter increased the thermal field and plastic flow, inhibiting defect generation at the cost of hardness reduction.

A relation of both shoulder and pin/probe diameters, with tools made of AISI 1040 carbon steel, with respect to the workpiece thickness reported in the literature is presented in Figure 6a for linear FSW, whereas Figure 6b depicts the relationship between the shoulder and pin/probe diameters for linear FSW. As expected, there are substantially more data regarding this topic for linear FSW than its orbital variant. In addition to that, it should be mentioned that in several published works concerning OFSW, a description of the tool used is not presented. It can be confirmed from the literature that the tools are similar in both variants of the process, meaning that no special dimension proportions are required for OFSW. The observed trends, in addition to being consistent, seem logical considering that by increasing the workpiece thickness, more energy input is needed; hence, a larger shoulder diameter is employed. Since it is assumed that there is a constant ratio between the shoulder diameter and the pin/probe diameter, it is also expected that the pin/probe diameter will increase as the shoulder diameter increases. Even though the most commonly used ratio of shoulder-to-pin diameter is 3:1, Fuller et al. [5] warned that there might be no general optimal ratio applicable for every material or thickness, meaning that an ideal tool ratio for a specimen of x mm in thickness might not be the same for a specimen of $2x$ mm in thickness. Considering that as the workpiece thickness increases, the thermal input of the shoulder decreases, the pin/probe must deliver more thermal energy. Moreover, materials with low thermal conductivity should not require a shoulder diameter as large as a material with a higher thermal conductivity.

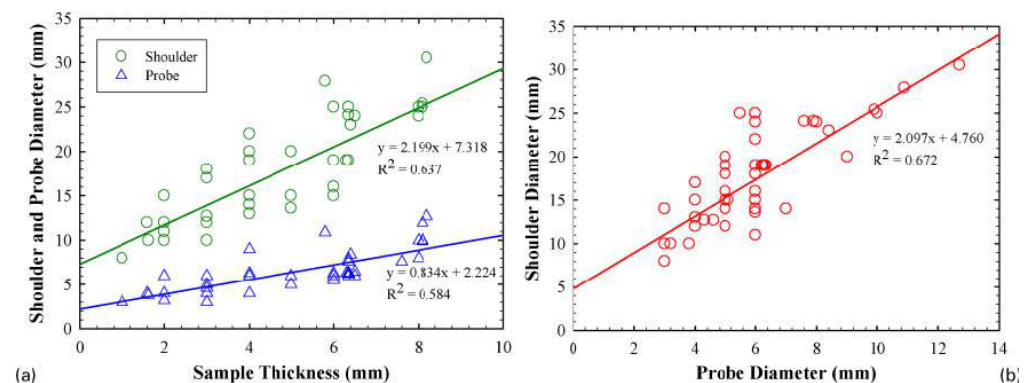


Figure 6. Linear FSW: (a) tool diameters versus workpiece thickness and (b) relationship between tool diameters, reprinted with permission from [21], 2023, Taylor & Francis.

3.1.3. Shoulder Shapes and Features

New shoulder features and geometries are constantly under development in order to improve process efficiency, not only by minimizing the applied forces intrinsic to the process or enhancing material flow and its containment, but also by maximizing the travel speed without compromising the weld quality. Even if they are small, these improvements in process efficiency can be very appealing to industry since they represent an impactful boost in productivity. Similar to tool materials, shoulder features and geometries are dependent on the variants of the process, materials to be joined or processed, and type of joint, so there is not a perfect tool for general application. The most common shapes and features of tool shoulders are presented in Figure 7.

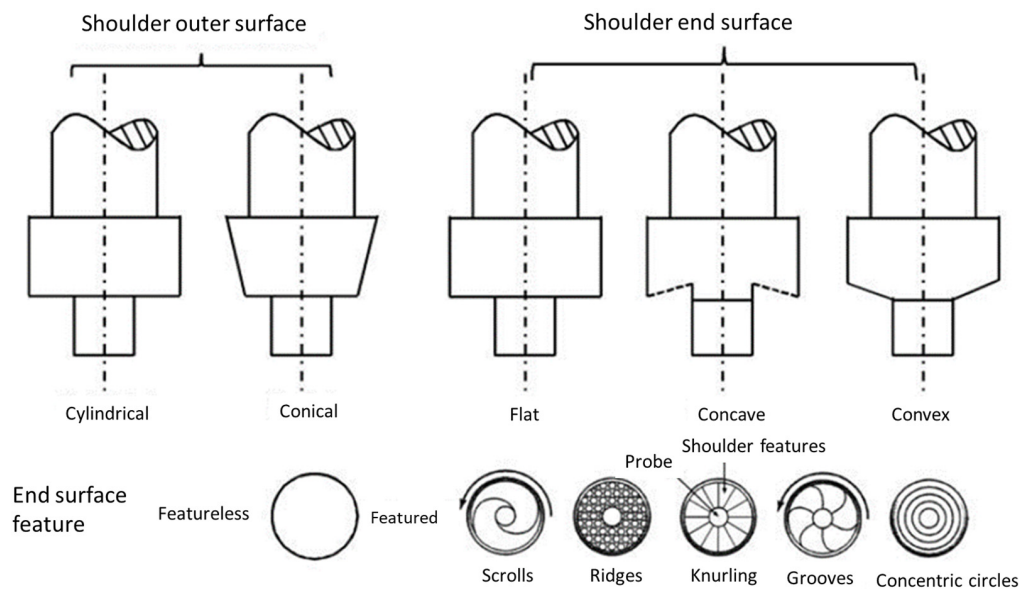


Figure 7. Most common shoulder shapes and features used in FSW, reprinted with permission from [21], 2023, Taylor & Francis.

As illustrated, the outer surface of the shoulder can be either cylindrical or conical. The most commonly used outer surface is cylindrical since the plunge depth is typically small (1–5% of the workpiece thickness). During the process, it is accepted that the outer shape of the shoulder has little influence on the weld quality, although there are reports of good-quality welds achieved by using a probe-free shoulder tool in which the outer shape of the shoulder may have an important role.

The flat end surface of the shoulder was the first and simplest geometry designed; however, it was found that this simple design was commonly related to the production of poor-quality surface welds, i.e., excessive flash, as a consequence of being inefficient in containing the flowing material under the shoulder. In the pursuit of enhancing the welding surface quality, the concave end surface was designed and rapidly became the most used thanks to its capability of containing the flowing material beneath it, thus limiting or avoiding the material extrusion from the border of the shoulder. This concave shape is not very steep, about 6–10° from the flat surface, so, depending on the tool material, the extra tool machining is easy to execute and is compensated by the improved results. The idea behind the concave shape is to serve as a reservoir for the displaced material from the probe, and as the tool moves forward, new material replaces the existing one, pushing it behind the probe. In order to maintain this reservoir along the path of the tool and consequently enable the compressive forging force on the weld generated by the trailing edge of the shoulder, the procedure requires a tool tilt angle of 1–3° from the normal, opposite the direction of travel. It has been reported that this leads to high hydrostatic pressures that may increase the integrity of the nugget. The remaining possible end surface of the shoulder is the convex one. Despite the seeming advantage of being able to maintain

full contact with the surface of the workpiece (lap joint/FSP) or both workpieces (butt joint), regardless of occasional variations in the specimen flatness and/or thickness, these tools are generally the least used in FSW/OFSW due to their tendency to push the material away from the probe, especially if no surface feature is adopted. However, there are reports of successfully produced welds with good quality on thin sheets.

Given the intent of optimizing the process and accomplishing higher-quality welds, surface features of the shoulder can be employed that have an impact on the material friction as well as the mixing of that material. The most prevalent profiles include scrolls, ridges, and grooves, among others, and are presented in Figure 7. According to the literature, scrolled shoulders are the most common for both FSW and OFSW applications. The purpose of the scrolled shoulder is to maximize the material containment from the edge of the shoulder during the tool rotation, benefiting from the elimination of using a tilt-angled tool [21]. Since in orbital applications, especially in small-diameter specimens, full contact between the shoulder and workpiece tends to be impossible, this shoulder feature reportedly increased the tolerances to the variations of the tool-workpiece contact [32]. In this study, the authors also performed OFSW on small-diameter pipes with a featureless shoulder, resulting in consistent poor surface quality and generating surface void defects as well as flash defects in contrast to what was observed when the scrolled shoulder was adopted.

3.1.4. Probe/Pin

As an essential section of an FSW/OFSW tool, the pin/probe is designed to disrupt the contact surfaces of the specimens to be joined, shear the material in front of the tool, and move the material behind the tool, producing deformational and frictional heating on those joint surfaces [5,21]. Over the years, different shapes and features on the pin/probe have been implemented to improve the flow of plasticized material and alter the weld properties; thus, travel speed, the extent of deformation, and the resultant microstructure of the welds are greatly dependent on the pin design [5,20]. Several of the most common pin/probe designs, shapes and variants found in the literature are presented in Figures 8 and 9. Despite the variety presented, it should be mentioned that not all of the viable pin/probe designs are mentioned in the open literature, as many of them are developed by the private industry, so those designs are contained in a patent or patent application [5].

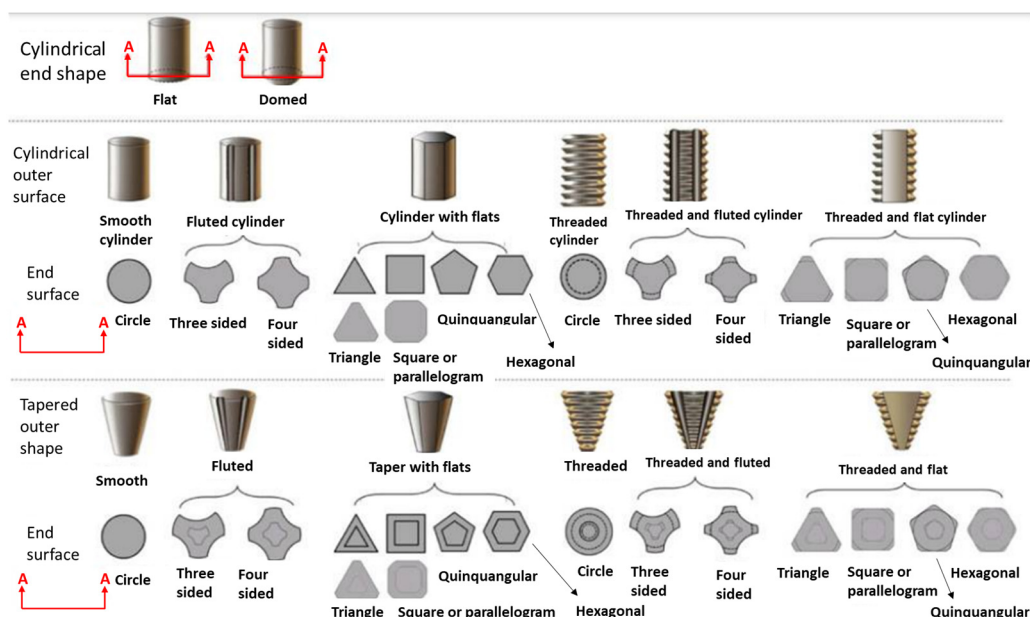


Figure 8. Pin/probe designs and shapes typically used in the friction stir welding process, reprinted with permission from [21], 2023, Taylor & Francis.

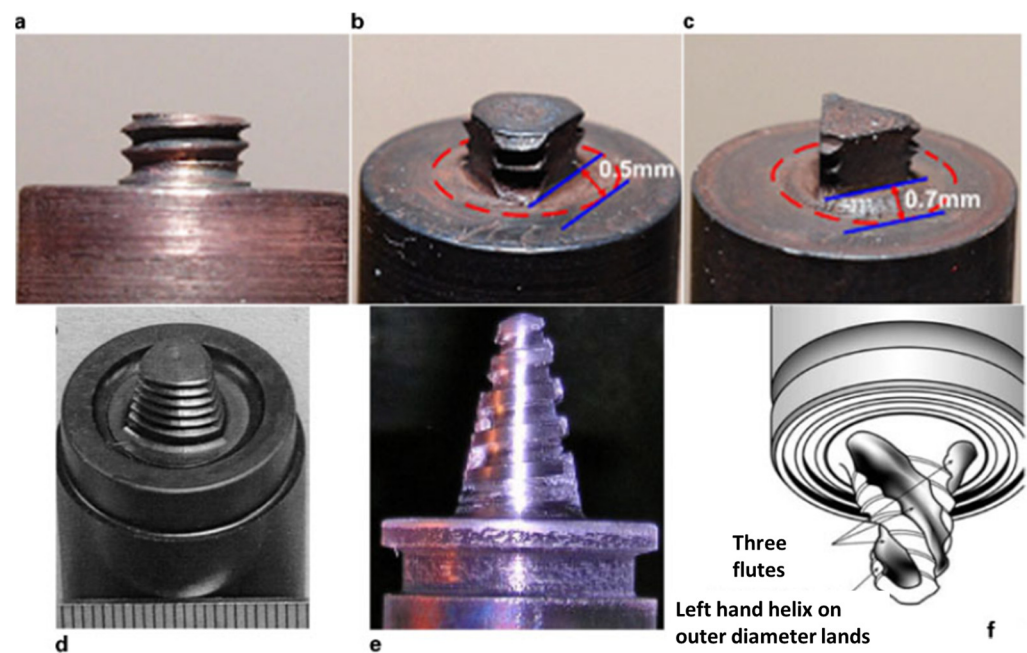


Figure 9. Pin variants used in FSW: cylindrical threaded (a), three flat threaded (b), triangular (c), Trivex (d), threaded conical (e) and schematic of a triflute (f), reprinted with permission from [20], 2023, Taylor & Francis.

As depicted in Figure 8, the end shape of an FSW tool can be either flat or domed. Originally, the pin/probe mentioned in the FSW patent by TWI [1] was a cylindrical threaded pin with a dome end shape. Although flat-end-shaped pins/probes have become the most commonly adopted due to their ease of machining, dome-shaped pins can significantly reduce tool wear during plunge and increase the tool life by decreasing local stress concentration, as well as improve the joining at the weld root [5,21]. The optimum dome radius has been reported as 75% of the pin diameter [32].

Regarding the outer surface of the tool pin/probe, it can be either cylindrical or tapered/truncated conical, and both can accommodate different shapes and features, such as threads, flats, or flutes. Indeed, earlier tools consisted of cylindrical pins/probes because they have been successfully producing good-quality welds of Al alloys up to 12 mm in thickness [5,21] and also due to their versatility since both the pin/probe length and diameter can be shortened if required [5]. However, as thicker workpieces, higher-strength alloys, and faster welding speeds started to gain more attention, truncated cone or tapered pins were developed, significantly reducing the transverse loads during the process. Not only are the transverse loads lower than in cylindrical pins/probes, but the highest moment load is also where it is stronger, i.e., at the base of the cone. This simple design innovation was crucial in preventing tool fracture during welding for those higher-thickness and higher-strength alloy workpieces. Despite those benefits, cylindrical pins are still extremely popular as they are perfectly capable of joining softer materials, and a great portion of the published work typically does not use very thick samples.

As previously mentioned, different shapes and features have been implemented on the tool pins/probes to improve the process by improving heat generation due to increasing the interfacial area, upgrading the material flow, or even influencing the forces inherent to the process. Threads have been the most adopted feature of FSW/OFSW tools [21]. For instance, if a clockwise tool rotation is applied, a tool with left-handed threads is required to allow the plasticized material to be transferred by the threads from the shoulder down to the end of the pin/probe along its surface [5,21]. Instead of being directly deposited behind the tool along the weld path, the threads make the flowing material circulate several times around the tool before being deposited, which can be deeply beneficial as it enhances material stirring, facilitates the closure of voids, and intensifies the oxide breakdown [21].

Threadless tools also have their uses, in particular when joining or processing high-strength or highly abrasive alloys that would rapidly wear away the threads. Instead of threads, tapered pin/probe tools can exhibit a stepped spiral profile, which has been developed for high-strength alloys where threadless pins could not guarantee enough material flow and threaded pins distorted during the process. Additionally, as mentioned before, for tool materials for high-strength alloys such as PCBN, machining threaded features is not easily feasible, hence the use of a stepped spiral on these tools [5].

Introduced by Thomas et al. [33], the presence of flat areas in the pin revealed a change in material movement around the probe, as these flats behave similar to paddles by increasing local deformation and turbulent flow of the plasticized material. By trapping the flowing material in the flats and then releasing it behind the tool, this feature promotes more effective mixing in addition to increasing the temperature across the workpiece thickness and expanding the weld nugget area [5,20,21]. The effect of flats on the transverse force and tool torque was studied by Colligan et al. [34], who concluded that a reduction in those forces was directly proportional to the number of flats on a tapered pin/probe. Instead of flats, flutes can be added to a threaded pin/probe, having the identical purpose of trapping the plasticized material downwards, granting faster welding speeds, better symmetry of the joint, and better mechanical properties [35].

In contrast to the early days of FSW, a better understanding of the material flow has enabled a considerable evolution of the tool geometry and the addition of more complex features aiming to further reduce the process loads and heighten the material flow and mixing. The Welding Institute (TWI) has been at the forefront of FSW/P innovation, developing tools such as WorlTM, MX TrifluteTM, Flared-TrifluteTM, and A-SkewTM tools, as well as some variants of these tools. For instance, both the WorlTM and MX TrifluteTM tools can produce welds of Al alloys up to 50 mm in thickness in a single pass at high welding speeds without compromising the weld quality due to their superior swept rate. The WorlTM tool differs from a tapered threaded pin/probe by exhibiting a helical ridge along the pin/probe surface, whereas the MX TrifluteTM was developed as a further refinement with three flutes cut into the helical ridge. The swept rate is an important parameter in tool design and stands for the ratio of the volume swept by the pin/probe during the tool rotation (dynamic volume) to the volume of the pin/probe itself (static volume). So, it seems intuitive that by adopting machining features such as threads, re-entrants, flats, and/or flutes into the probe/pin, a higher swept rate is achieved. For comparison, Zhang et al. [21] reported that when welding a 25 mm thick plate, the swept rate of a typical cylindrical probe was 1.1:1, whereas for WorlTM and MX TrifluteTM tools, it was 1.8:1 and 2.6:1, respectively. A significant reduction in the displaced volume by using these tools (60% and 70% for WorlTM and MX TrifluteTM, respectively) results in a reduction in the transverse loads, enabling even faster welding speeds.

TrivexTM tool probes consist of three convex sides to inhibit the entrapment of flowing material. Flared-TrifluteTM and A-SkewTM probes were developed as a more viable alternative to performing FSW in T and lap configuration since using conventional cylindrical threaded probes/pins often resulted in a serious thinning of the upper plate, damaging the workpiece's bending properties. In addition to reducing the axial forge forces and consequently decreasing the thinning of the upper plate, these tool probes allow faster welding speeds and also promote a significant widening of the weld region.

Table 2 summarizes the type, material, shapes, and features of FSW tools used in some published studies on OFSW.

Table 2. Tool type, material, shape, features, and welding parameters used on published work for OFSW.

Workpiece Material	Type of Joint	Type of Tool	Tool Material	Shoulder Shape, Features, and Geometry	Pin Geometry, Shape, and Features	Remarks about Tool	References
AA5456-O (2.5 mm thickness) AA5456-H321 (5 mm thickness) D: 370 mm	OFSW (lap joint)	Fixed	H13 Tool Steel	Flat Featureless SD: 20 mm	Tapered Triflute Pin PTD: 7 mm PBD: 6 mm PL: 6, 7, and 8 mm	A PL of 6 mm revealed poor bonding. The triflute pin improved material flow.	[36]
AA5083-H321 (5 mm) AA5083-O (2.5 mm) D: 360 mm	OFSW	Fixed	H13 Tool Steel	Flat Featureless SD: 21 mm	Triangular Frustum PTD: 7 mm 4 mm side at the bottom PL: 7 mm		[37]
AA6063 (5 mm) D: 89 mm	OFSW (butt joint)	Fixed	High-carbon Steel	SD: 20 mm	Cylindrical PD: 5 mm PL: 3.8 mm	Offset: 6 mm	[38]
AA6063-T6 (5 mm) D: 89 mm	OFSW	Fixed	H13 Tool Steel	SD: 20 mm	Cylindrical PD: 5 mm PL: 3.8 mm		[39]
AA6061-T6 (5.1 mm) D: 107 mm	OFSW	Fixed		Flat Scrolled SD: 15.9 mm	Cylindrical Threaded PD1: 4.8 mm PD2: 6 mm PL: 4.572 mm	The scrolled shoulder and offset of 6 mm allowed for good-quality welds in small-diameter pipes.	[32]
AA3003 (1.5 mm) Pure Cu (1 mm) OD: 19 mm	OFSW	Fixed	H13 Tool Steel	Concave (10°) SD: 6 mm	Cylindrical PD: 2 mm PL: 0.7 mm		[40]
AA6061-T6	OFSW	Fixed	High-Speed Steel	SD: 20 mm	Conical PTD: 5 mm PBD: 3 mm PL: 4.2 mm		[41]
AA6060-T6 (5 mm) D: 80 mm	OFSW	Fixed	AISI 1040	SD: 20 mm	Conical PTD: PBD: 5 mm		[42]

Table 2. Cont.

Workpiece Material	Type of Joint	Type of Tool	Tool Material	Shoulder Shape, Features, and Geometry	Pin Geometry, Shape, and Features	Remarks about Tool	References
AA6063-T6 (5 mm) D: 100 mm	OFSW	Fixed	AISI 4140 Steel	SD: 20 mm	Left-hand-threaded PD: 5 mm PL: 5 mm		[43]
	Spiral Weld						[44]
AA6082-T6 (3.5 mm) OD: 38 mm	OFSW	Adjustable Pin Tool	X40CrMoV5-1 and DIN 1.2344 Vacuum heat-treated and double-tempered (HR _C 54)	Concave (6°) SD: 10 mm	Threaded PD: PL: 200 mm (adjustable)		[22]
Commercial Pipeline Steels X65–X120 (16–19 mm) D: 762 mm	OFSW Two-sided welds (11–12 mm each)	Fixed	Tool 1: PCBN Tool 2: W-Re	Tool 1: “Traditional design” Tool 2: “Continuously tapered pin and relatively small shoulder”			[45]
AA6063 API Grade X65, X80, X100, and L80 Steels (13 mm) ID: 305 mm	OFSW	Fixed			Tapered Pin		[17,46]
AA6061							[47]
X42 Carbon Steel (12 mm) OD: 320 mm	OFSW	Fixed	PCBN-based Tools (Q60: 60 wt/% cBN and 40 wt/% WRe)	Convex Step Spiral	Tapered Threaded		[26]

D: Diameter; OD: Outside Diameter; ID: Internal Diameter; OFSW: Orbital Friction Stir Welding; OFSLW: Orbital Friction Stir Lap Welding; SD: Shoulder Diameter; PD: Pin Diameter; PTD: Pin Top Diameter; PBD: Pin Bottom Diameter; PL: Pin Length.

By critically interpreting not only Table 2 but also other published work about OFSW, a few notes should be made. Some authors do not describe the tools used, neglecting the influence that the tools have on FSW/OFSW procedures. The use of simpler and traditional tools instead of those with features that are proven to improve the quality of welds is widespread across the literature. This is reasonable work that was published before these advancements; however, for recently published studies, budget limitations of research facilities might prevent them from acquiring new and more appropriate tools for every new application, which can be understandable. Nonetheless, the trend of more recent studies has been to adopt these tool features or even evaluate the different benefits derived from each of them. For example, regarding the selection of the tool's material, steel should be used for low melting temperature alloys, such as Al and Mg, and PCBN or W-Re tools should be used for high melting temperature materials, such as titanium and steel alloys.

3.2. Equipment Requirements for Orbital FSW

Similarly to linear FSW, milling machines [38,48–51], custom-built or dedicated FSW machines [52], and industrial robots [53–55] are the three kinds of machines that seem viable to conduct OFSW, according to the literature.

When welding high-strength materials, such as steel, stainless steel, titanium, and nickel alloys, that require high load supports [56], elevated robustness is needed. The use of custom-built or dedicated FSW machines presents some advantages over the others since these dedicated FSW machines tend to have the highest load capability, stiffness, accuracy, and availability [52], hence their use to weld high-strength materials should be more suitable. In addition, given the versatility of their configurations, dedicated FSW machines can be used on long, small, thick, and thin workpieces, as well as applications that require high stiffness, and can also be used in single- or multi-axis applications. However, these dedicated machines tend to be expensive, and if more flexibility is needed, their cost also increases. In general, this type of machine is associated with high-series production and is more suitable for industrial applications, such as the tailored welded blanks of the automotive industry [57].

Welding applications that require 3D weld paths, such as OFSW, are becoming more attractive and possible to accomplish given the recent developments in the robot industry. Previously, the lack of load capability and low stiffness of articulated robots prevented their use in most FSW applications; however, since these recent developments in the industry, it has become possible to join aluminum materials up to 6 mm in thickness using these machines. There are, essentially, two categories of industrial robots capable of performing FSW/OFSW: articulated arm robots and parallel-kinematic robots.

The use of articulated arm robots sounds advantageous for some applications not only because of their high flexibility and 5 to 6 degrees of freedom but also because of their process automation potential, which can lead to productivity improvements. However, due to the low stiffness of these machines and the relatively high loads required in the FSW process, several FSW/OFSW applications might be limited or even impossible, such as titanium welding. In order to achieve this level of flexibility and DOF, arm robots are a combination of several joints and links composed by a series of servo motors, gearboxes, and transmissions in which there is always some backlash and/or vibrations, resulting in deflections of the machine that are not countable by the encoders, leading to deviations from the welding path and decreasing its accuracy as long as load requirements increase. Another option for robotic FSW/OFSW is the parallel-kinematic robots, which, in addition to the automation capabilities of the articulated arm robots, are more robust and present higher stiffness; however, flexibility and range of orientation are compromised, as is the price, which is significantly higher than articulated arm robots. A concept of an adaptation of an articulated arm robot has been developed by Mendes et al. [54] and is illustrated in Figure 10. They reported that the apparatus was successfully used to produce FSW on polymeric materials; however, it was not demonstrated on metallic materials.

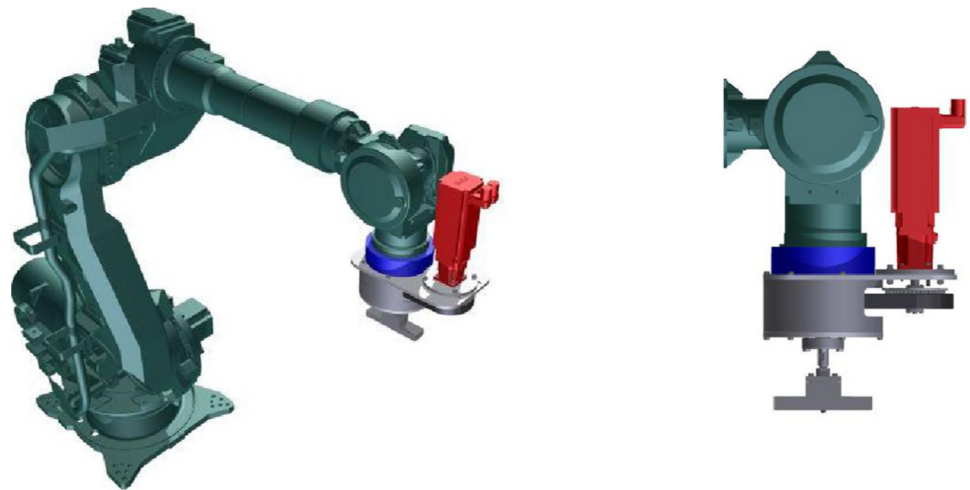


Figure 10. Articulated arm robot adapted for FSW, reprinted with permission from [54], 2023, Springer Nature.

The use of industrial robots, modified articulated arm robots, or parallel-kinematic robots for complete orbital welds on applications such as fuel tanks or pipes requires the most space, a well-supported workpiece, and no obstructions along the path of the robot. If the robot is stationary, meaning that the travel speed is promoted by the rotation of the workpiece instead of the robot's motion, it would be more appropriate to use a standard milling machine instead.

The use of a standard milling machine tends to be more associated with research in universities since most of the mechanical engineering departments own at least one for machining applications; hence, most of the published work on OFSW uses this equipment. Milling machines are appealing in applications that require high stiffness or high temperatures, such as titanium or steel, and are ideal for prototyping and small-series production since some modifications can be implemented into the machine, increasing its flexibility. Therefore, for research activities and given the limited budget inherent to universities when compared with dedicated industries, the purchase of a dedicated FSW/OFSW machine usually does not compensate. Linear FSW performance does not depend upon many adaptations other than effective clamping; however, when using a standard milling machine for an OFSW procedure, such as the joining of tubes or cylindrical workpieces, some apparatus is required to be incorporated into the milling machine not only as a holding mechanism for the workpieces to be joined, supporting all the forces and torques inherent to FSW, but also to be responsible for the rotation of the workpiece at a constant speed (travel speed) beneath a rotating stationary tool of the milling machine. This apparatus is referred to as the "Orbital Clamping Unit" [58]. When designing this clamping device, several characteristics of the process, such as torque, spindle speed, plunge load, transverse load, and slide force, should be evaluated and quantified, as it must support all the forces inherent to the process. In most published work that uses this apparatus, the travel speed parameter is promoted by the rotation of the workpiece or tube. In order to promote that rotation, typically a servo or DC motor must be incorporated into the apparatus. So, the first step is to choose, based on calculations and the literature, a suitable motor with enough torque and rotation speed to perform OFSW. Ideally, the motor specifications should be overdimensioned to avoid working near the motor's limit, especially regarding torque. Furthermore, the motor rotation should be easily and precisely adjusted, not only to optimize the process but also to enhance its reproducibility. Following the motor choice, the apparatus should be conceived and produced. For academic purposes, the system should be easily adapted to fit different sizes of tubes and rods. In the case of joining tubes, the apparatus must be stiff enough to maintain full contact between specimens during the plunge stage, as well as mitigating any possible vibration promoted by the tool spindle that will greatly affect the weld quality.

In summary, none of the equipment types is without drawbacks; therefore, some compromises must be established. A general comparison of FSW equipment types is presented in Table 3.

Table 3. Comparison of FSW equipment types and features, reprinted with permission from [55], 2023, Elsevier.

Characteristics	Equipment			
	FSW Machine	Articulated Robot	Parallel Robot	Milling Machine
Flexibility	Low/Medium	High	High	Low
Cost	High	Low	High	Medium
Stiffness	High	Low	High	High
Work volume	Medium	High	Low	Medium
Setup time	High	Medium	Medium	Low
Number of programming options	Medium	High	High	Low
Capacity to produce complex welds	Medium	High	High	Low
Control type	Motion/Force	Motion	Motion	Motion

Despite the chosen equipment to perform OFSW, certain features intrinsic to the process should not be neglected, namely the backing support, which is always required not only in OFSW but also in linear FSW, and the commonly referred to keyhole “defect.” The “keyhole,” as the name suggests, is the hole left in the workpiece by the tool removal process after the welding process is completed. Although it compromises the integrity and quality of the welding process, characterizing the “keyhole” as a defect can be ambiguous since it is more a characteristic of the process than a defect that can be mitigated by parameter optimization. When performing linear FSW, avoiding the keyhole is simpler than during the orbital variant since the typical solution is to overdimension the plates or sheets to be joined or processed and cut the excess part where the keyhole is located. Despite being more complex to execute, evading the keyhole in the OFSW process can and should also be conducted, and a few solutions are proposed. Due to the impossibility of cutting the excess part on tubular specimens, Mahoney et al. [26] developed a tool run-off ramp (Figure 11) to avoid the keyhole in the workpiece, which is the most popular solution, although it slightly increases the complexity of the apparatus. It should be noted that not only is the keyhole a weak point in the weld, but the beginning can also put the workpiece in jeopardy. To solve this, there should be a slight overlap ($\sim 40^\circ$) of the tool passage. When using the tool run-off ramp, it should be in contact and tangent with the workpiece, and, as the orbital motion stops at $\sim 40^\circ$, depending on the equipment used (orbital motion of the tool or the workpiece), a linear FSW begins from the workpiece into the tool run-off ramp, leaving the keyhole in the ramp instead of the workpiece. While this transition occurs, the welding parameters should be adjusted in order to increase the heat input. After the process is complete and the tubular specimens are joined, the run-off ramp is removed by grinding, thereby increasing the waste material as well as the time consumption, which can be a constraint in certain industrial environments. Another solution to the problem, although less used in research, is to adopt the retracting pin tool patented by NASA [26], which retracts the pin in a controlled manner after the completion of the travel motion, allowing the keyhole closure. In this work, the retraction time of the pin was 5 s. This tool can be very useful and advantageous, especially in the orbital variant of the process, since no modifications are required in the apparatus and no material is wasted by grinding, in addition to needing less time to achieve good-quality results. Figure 12 shows a situation where the keyhole was eliminated using this specific tool. However, similar to any type of equipment, it is not perfect and can be less favorable than the run-off ramp due to its higher cost and more expensive controlling systems. Furthermore, when using the run-off

ramp, any suitable standard tool is able to perform OFSW. It has also been reported that the keyhole can be successfully sealed by filling it with, if possible, the same material by fusion methods, although for alloys such as the AA6XXX series, this solution tends to be difficult to execute and is susceptible to defects, as previously stated in the “Advantages and limitations of solid-state welding over fusion welding” chapter.

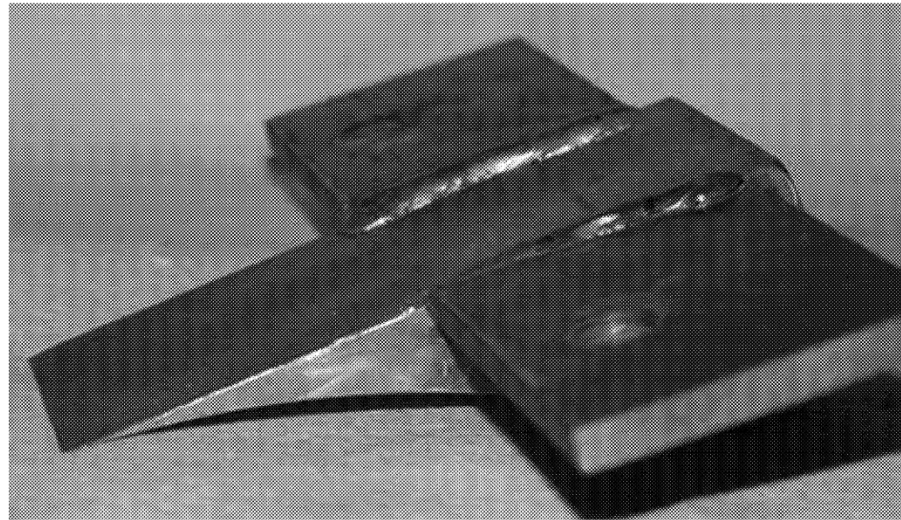


Figure 11. Example of a run-off ramp used in FSW and variants, reprinted with permission from [26], 2023, Springer Nature.

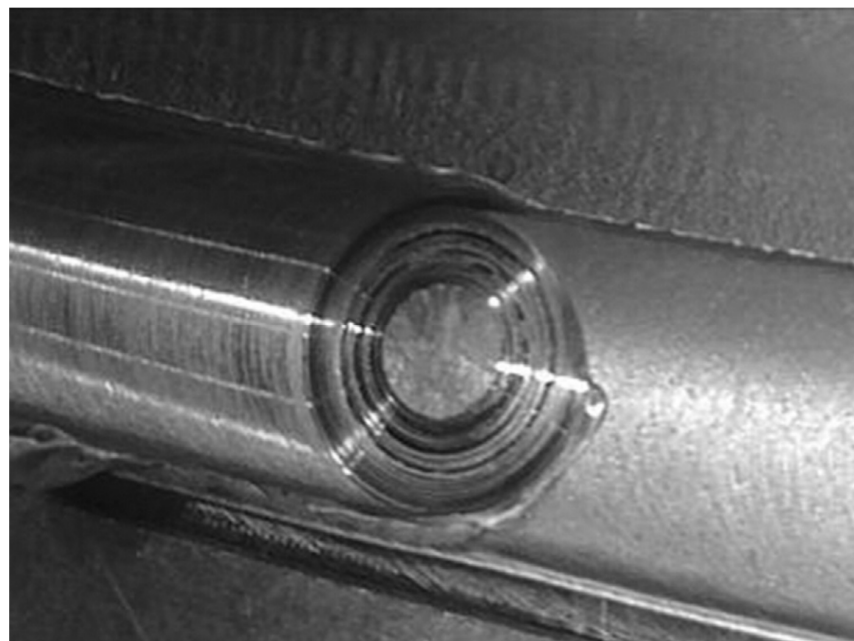


Figure 12. Elimination of the keyhole using a retractable pin tool, reprinted with permission from [59], 2023, Elsevier.

The other characteristic of the process that should be mentioned in this chapter is the demand for backing support, which is a requirement to avoid workpiece collapse both in linear FSW and its orbital variant. Similar to the keyhole issue, the backing support tends to be easier to apply in linear FSW as it is commonly used with a harder material plate that is in full contact with the plates or sheets to be joined or processed. When performing OFSW, the same principles are applied, although executed differently due to the tubular nature of the workpiece. As discussed in the tools chapter, a self-react or bobbin

tool can be used to improve the backing support in the case of joining tubular specimens; however, maintaining an adequate contact between the tool shoulder and workpiece that promotes enough material containment can be hard to achieve due to the necessity of the tool being perpendicular to the specimen surface. Thus, it is not possible to employ a tool tilt angle or the commonly adopted tool offset, which, as will be addressed later, works similarly to the tilt angle, making this type of tool rarely used in OFSW. Most of the published works report performing OFSW on tubular specimens of a constant diameter, as the solution tends to be the simplest. In this case, the backing support derives from an internal tube or rod of a harder material attached to the apparatus, with an outside diameter as close as possible to the inner diameter of the tube specimen to be joined or processed in order to maintain the needed full contact between the surfaces. However, this simpler solution has its drawbacks. Both the insert and removal of this internal backing support (mandrel) can be difficult to execute, as the gap between the surfaces should be as close as possible to zero to avoid undesirable deformation of the workpiece, such as turning it into an oval shape. To quantify the deformation promoted by the axial forces without the backing support, Lotpy et al. conducted several experiments under various parameters, achieving a minimum deformation of 1260 μm in a butt joint using a square pin profile at 1700 rpm and deformations as low as 542 μm in a stepped joint using the same square pin profile at 910 rpm [60]. So, an expandable mandrel can be a viable solution since it not only promotes an easier insert and removal for constant-diameter tube specimens but may also be the only solution for tubular specimens with a variable diameter. These internal mandrels, in contrast to the tube or rod mandrel, usually only support the zone of the tool passage; hence, they are mandatory to the apparatus system, thus simplifying it. The most critical constraint, rarely performed on research work but instead part of industrial applications, is if the workpiece is to be sealed or almost sealed, such as a fuel tank, which is becoming increasingly common in the aerospace industry. If the workpiece is to be almost sealed, a solution can be to use a lower melting temperature material as a mandrel that can withstand the axial forces without deformation. After the process is complete, the workpiece is heated, melting the mandrel material, which then leaks out of the workpiece. This solution, however, can alter the workpiece's condition, such as its temper, which is important to consider. In the case of welding or joining two parts for the workpiece to be fully sealed, this cannot be possible. So, if there are no issues with leaving the mandrel inside the workpiece for a specific application, that is what should happen. However, if leaving the mandrel inside the workpiece is not possible, some adjustments in one of the parts to be joined must be executed, as it is always required to have backing support underneath the joining line. One of the parts should not have a tubular form but instead a rod-like form, mainly in the welding zone. An example is presented in Figure 13, where not only a butt-joint but also a lap-joint is performed, reinforcing the union between the two parts.

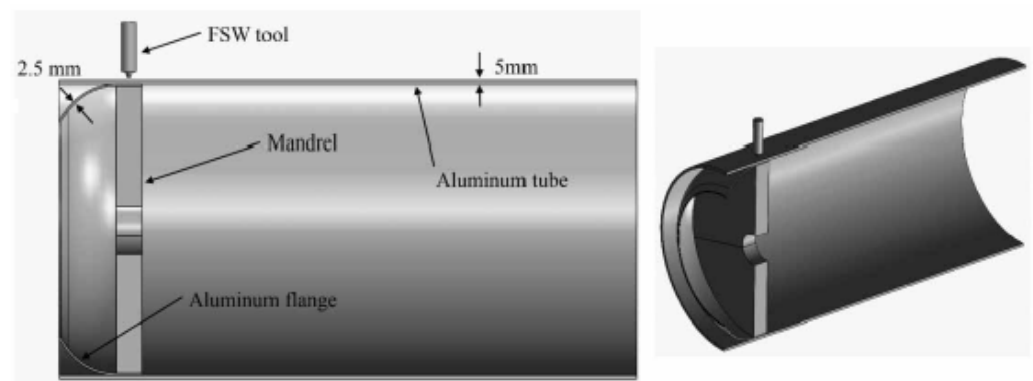


Figure 13. OFSW in a lap-joint application, reprinted with permission from [37], 2023, Taylor & Francis.

3.3. Materials

Since there is no fusion or filler material in the FSW process, it is possible to join a wider range of materials than in conventional fusion welding, as the compatibility of the composition of the materials to be joined is not a requirement like in conventional fusion welding [5]. Given that, materials such as high-strength aluminum, which are difficult to weld by conventional methods due to their high conductivity and reflectivity [9], can be joined effectively. Regarding linear FSW, there is vast research and published work on successfully joining diverse aluminum, magnesium [61], copper, titanium [62–64], and steel [65–70] alloys, as well as dissimilar materials. However, as expected, published work related to OFSW is much more limited, although there are reports of successful welds on tubular specimens, mainly composed of aluminum [22,37,42,49,71–73], steel [17,45,74], titanium [63], copper, magnesium, or zinc alloys, and also dissimilar materials (AL3003 and pure copper) [40]. FSW/OFSW performed on aluminum alloys that are considered non-weldable, such as the AA6XXX series, tend to be the main focus material of published work, which is understandable given the superiority of FSW/OFSW over the fusion methods for these alloys, filling an industrial “void” after so many years. However, in recent years, as tools and equipment have improved, harder materials have received more attention. For instance, Kumar et al. [45] report successful orbital welds in pipe steels up to 19 mm in wall thickness using a double-sided FSW procedure using both PCBN and W-Re tools.

Unlike aluminum alloys, which are difficult to fusion weld, as previously stated, titanium and steel alloy welds can be conducted by fusion techniques, achieving highly efficient results [5]. Therefore, unless academic or research work is intended, the benefits of performing FSW/OFSW on these materials should be evaluated since highly robust equipment is demanded in addition to the more expensive and less durable tools required.

3.4. Process Parameters

Both in linear FSW and OFSW, it is advised to carefully monitor the forces, torque, and temperatures, in addition to the more typical monitored rotation speed and travel speed, if good quality welds and reproducibility are intended, both of which tend to be neglected as their monitoring is difficult to execute and complementary equipment is mandatory.

Usually, the optimization of the parameters is performed empirically since the geometry of the joint, workpiece dimensions, material, and FSW machine have a great influence on the quality of the weld.

Nonetheless, the first step to optimizing the process is usually conducted by adopting different relations between the rotation speed ($\Omega = \text{rev} \cdot \text{min}^{-1}$) and the travel speed ($v = \text{mm} \cdot \text{min}^{-1}$). These ratios can be classified as “hot FSW conditions” if their value is above four, and “cold FSW conditions” if they are under two. Any values between two and four should be classified as “intermediate FSW conditions.” These classifications were established for the author’s proposed model, iSTIR [75]. Note that the same ratio value can be obtained with different sets of those parameters. This distinction was made due to differences observed in their macrostructure, hardness field, and temperature measurements. Furthermore, the main difference between these conditions, according to the author, lies in their heat flow, as for the cold FSW conditions, the heat is mostly derived from the extensive plastic flow deformation promoted by the pin action as the material is transported around the pin from the advancing side to the retreating side, where the heat is dissipated, i.e., viscous dissipation. In contrast, since in hot FSW welds the heat generated by the interfacial friction between the tool and workpiece is higher and most of the plastic flow deformation occurs near the pin, the distribution of the generated heat tends to be similar for both the advancing and retreating sides.

When joining tubular specimens, especially those with small diameters, it is evident that the contact between the tool shoulder and workpiece is significantly different from a plate butt joining configuration unless an enormous plunge depth is promoted, which is dependent on the diameter of the workpieces to be joined and may not be feasible in the case of low-thickness specimens. Given that the contact between the tool shoulder

and workpiece is critical for heat generation by friction and also responsible for material containment, problems might occur during the process if its contact with the workpiece is not adequate. The relationship between weld conditions, heat generation, temperature, and friction coefficient can be summarized in the relationship map shown in Figure 14.

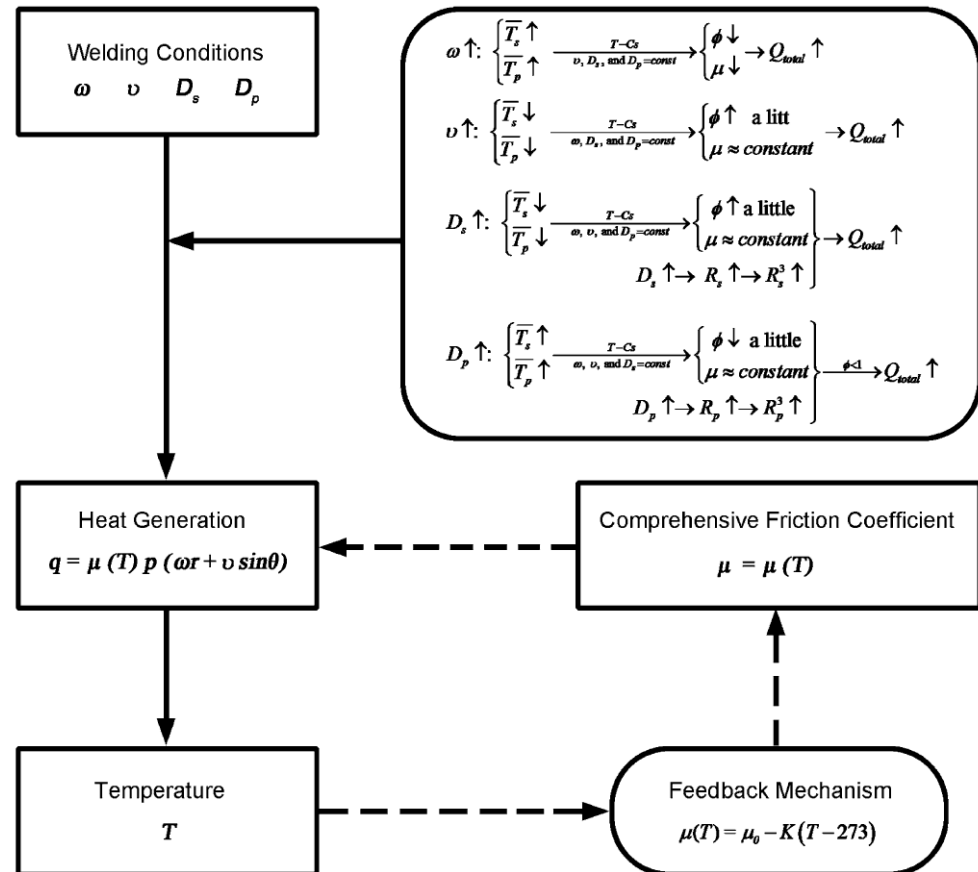


Figure 14. Relationship between the welding parameters and temperature for FSW 6061Al, reprinted with permission from [30], 2023, Springer Nature.

Lammlein et al. [32] reported that positioning the FSW tool directly above the highest point of the pipe resulted in a bumpy and unstable weld condition. They found empirically that a tool offset of 6 mm was ideal for pipes with a 107 mm diameter and greatly improved the joint quality. The adoption of an offset creates an effect similar to the tilt angle commonly used on linear FSW, meaning that the trailing edge of the tool shoulder is the portion deepest in the workpiece, improving the role of the shoulder in material containment and heat generation. It has also been reported that the possibility of wormhole defects can be mitigated when an appropriate offset is employed [71]. The use of an offset instead of a tilt angle has been generally accepted as the improvements in weld quality have been proven and reported.

Furthermore, when performing FSW/OFSW of dissimilar materials, another type of offset has also been reported to be effective as an approach to prevent the formation of tunneling defects, which consists of positioning the tool towards the weaker material [76]. As an example, Muthu et al. [77] reportedly produced defect-free dissimilar welds of AA1100-14 and pure copper while applying a 2 mm offset of the centerline to the aluminum side.

Given the empirical nature of the parameter optimization previously stated, the majority of the published work regarding OFSW consists of or includes a comparison between various combinations of those parameters, most commonly the rotation speed and travel speed. The influence of the remaining parameters, such as plunge depth, axial force,

tilt angle, and offset, has also been reported and evaluated. For instance, by employing Taguchi methods and consequent ANOVA performance, Ganapathy et al. [78] concluded that for a linear FSW of two AA6063-T6 plates and using a tool with a straight cylindrical pin, the most significant contribution to the overall response was the axial force (48%), whereas travel speed and rotation speed contributions were 22% and 1%, respectively. Note that for the OFSW variant, such an in-depth study has not been performed yet.

Intuitively, the process parameters are highly dependent on the material to be welded, considering the differences in their intrinsic properties. However, the optimization of the parameters requires not only bearing in mind the material, its condition (heat-treated, residual stresses), and its dimensions but also considering the type of joint (butt joint or lap joint), the tool's material, geometry, and dimensions, and applied forces.

3.5. Joint Characterization

The quality of the welding process, or even of any mechanical processing technology, can only be qualified and quantified by characterizing the obtained workpieces. As a general rule, the more characterization methods performed, the better, as there is no such thing as “too much information.” In this section, the techniques that will be addressed are macro and microstructural evolution, tensile strength, and microhardness, since published studies tend to be mainly focused on these methods and can present a decent overall estimate of the properties of specimens. However, if industrial applications are intended, additional characterization techniques such as fatigue testing, corrosion behavior, eddy currents, XRD, and a vast array of other advanced characterization techniques should be conducted. An interesting and detailed overview of what has been tested for linear FSW was presented by Mishra et al. [5].

Upon completing an OFSW process, the first method to estimate and evaluate the quality of the weld or processing relies on visual inspection, since some defects can be visible at the specimen's surface or even its appearance can be a good first indicator of good quality welding. This is particularly useful when comparing different sets of parameters, which tends to be the case for most of the published work. Figure 15 presents a comparison of the surface appearances obtained from OFSW while adopting different sets of parameters. By visual inspection, one can assume the superior quality of samples 2 and 3, although additional characterization should be performed to validate these claims. In sum, visual inspection is an excellent first step as it requires minimal time and preparation.



Figure 15. Visual inspection of the surfaces obtained from OFSW, reprinted with permission from [22], 2023, Elsevier.

3.6. Microstructural Evolution

Microstructural transformations are intrinsically related to alterations in post-weld mechanical properties, being a consequence of the induced severe plastic deformation and also the high-temperature exposure of the workpiece during an FSW/OFSW procedure. By the characterization of grains as well as precipitate distribution, three distinct zones in addition to the base material (BM) zone are identified that are similar in both the orbital and linear variants of FSW, namely the stirred zone (SZ) or nugget, the thermo-mechanically-affected zone (TMAZ), and the heat-affected zone (HAZ).

The stirred zone, known as the weld nugget, similar to in fusion welding, is where the actual joining happens. This zone easily distinguishes itself among the others by exhibiting a recrystallized equiaxed fine-grained microstructure resultant of the intense plastic deformation and frictional heat during the FSW/FSP (as well as their orbital variants) process, hence also being referred to as the dynamically recrystallized zone (DXZ). Generally, inside the recrystallized grains of the SZ, there is a low dislocation density, although contradictory claims have been reported as well as reports of it containing a high density of sub-boundaries and sub-grains. Furthermore, under certain process conditions, the SZ can display an onion structure, and its shape is also influenced by the process parameters, typically revealing a basin shape for the lower tool rotation speeds and a more elliptical shape when higher rotations are employed. In both cases, it has a sharper interface with the TMAZ on the advancing side over the retreating side of the tool, where the author [32] compares different sets of parameters while maintaining the tool in tubular specimens of AA6061-T6, which is more evident when comparing the 1200 rpm specimens with the 1600 rpm ones.

Regarding the size of the recrystallized grains of the nugget zone, they are commonly in the microrange ($<20\ \mu\text{m}$ for most of the aluminum alloys), although ultra-fine grains of $<1\ \mu\text{m}$ have also been achieved in linear FSW by external cooling [79], acting as a limitation of grain growth derived from high-temperature exposure. Furthermore, the grain size is not constant across the SZ, with larger sizes in its upper region because it is closer to the shoulder of the tool and reaches higher temperatures derived from friction than the lower region. In the lower region, lower temperatures and shorter thermal cycles are attained since heat dissipation by conduction into the workpiece and the backing support (backing plate for linear FSW and inner mandrel or tube in OFSW) occurs during the process, thus causing a larger gradient of the grain size as the thickness of the workpiece increases. Despite different methods of dynamic recrystallization that have been proposed, the one that seems to be the main mechanism for recrystallization during the process in aluminum alloys is discontinuous dynamic recrystallization (DDRX), since the recrystallized grains in the SZ tend to be significantly smaller than the pre-existing sub-grains in the parent material. Additionally, given that temperatures in the SZ can surpass $500\ ^\circ\text{C}$ in combination with the intense plastic deformation, both coarsening and dissolution as well as reprecipitation of the strengthening precipitates have been reported to occur in this zone when compared to the base material.

The TMAZ is categorized by exhibiting elongated grains in an upward-flowing pattern around the nugget. This transition zone is not observed in fusion welding, being unique to the FSW/FSP process. Despite revealing a highly deformed structure that underwent plastic deformation and high-temperature exposure, recrystallization similar to the nugget zone is not usually observed in the TMAZ due to insufficient strain. However, the high-temperature exposure in this zone is enough to promote not only the growth of grains but also the dissolution of some precipitates present in the base material, to a degree depending on the experienced thermal cycle. Additionally, it has been reported that these deformed grains typically contain a high density of sub-boundaries.

The HAZ is the last zone affected by the process, parent to the TMAZ and BM, exhibiting a microstructure similar to the latter since there is no plastic deformation in this zone. However, as suggested by its name, this zone is indeed affected by high-temperature exposure, revealing overall grain growth as well as an impact on the precipitate structure.

The precipitate structure changes can greatly compromise the mechanical properties, in particular for the heat-treatable aluminum alloys, if the thermal exposure exceeds 250 °C, as it has been reported that it results in coarsening of those strengthening precipitates and, therefore, increasing the precipitate-free zone by a factor of up to five.

The BM zone, as the name suggests, is the zone from which the initial properties are maintained, meaning that despite the workpiece being exposed to an increment of temperature by conduction, this increment is not sufficient to promote any microstructural or precipitate structure changes in the material. A summary of these zones in microstructural evolution and the main aspects are depicted in Figure 16. Additionally, in Figure 17, these zones are exposed in a macrograph with identification of the process's retreating and advancing sides.

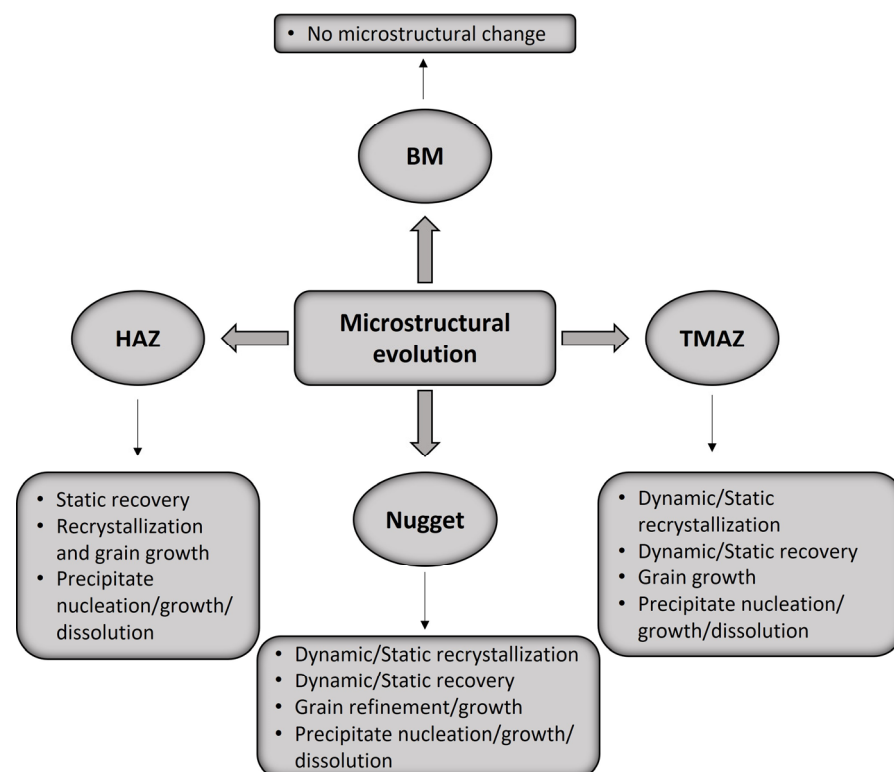


Figure 16. Microstructural evolution, zones, and important aspects, reprinted with permission from [80], 2023, Springer Nature.

Given that adopting a retractable pin tool is a viable solution to avoid the keyhole in OFSW procedures, Gibson et al. [81] intended to identify the microstructural differences promoted by the retraction of the pin, revealing interesting results. Not only was the TMAZ affected, exhibiting a vortex-like shape, but also the upper region of the nugget was revealed to be more symmetric with a horizontally layered microstructure as a consequence of different strain ratios of the keyhole filling due to the upward movement of the tool.

3.7. Common Defects

When comparing FSW with conventional fusion welding, it is true that most of the defects caused by the latter, such as porosities, hot cracks, loss of alloying elements, and loss of mechanical properties, may not be present in FSW; however, the FSW process is also not free of defects. A schema displaying some of the most common defects as a function of the main process parameters (rotation and advancing speed) is presented in Figure 18. These defects are usually related to the process parameters and can be easily mitigated by their optimization [82]. It should be noted that the tool rotation and advancing speed are not isolated in the heat input contribution, as the applied pressure or even the tool design also

have an impact on that heat contribution. Generally, defects such as void formation and nugget collapse tend to occur as a consequence of extreme heat input caused by adopting a high rotation speed relative to the advancing speed.

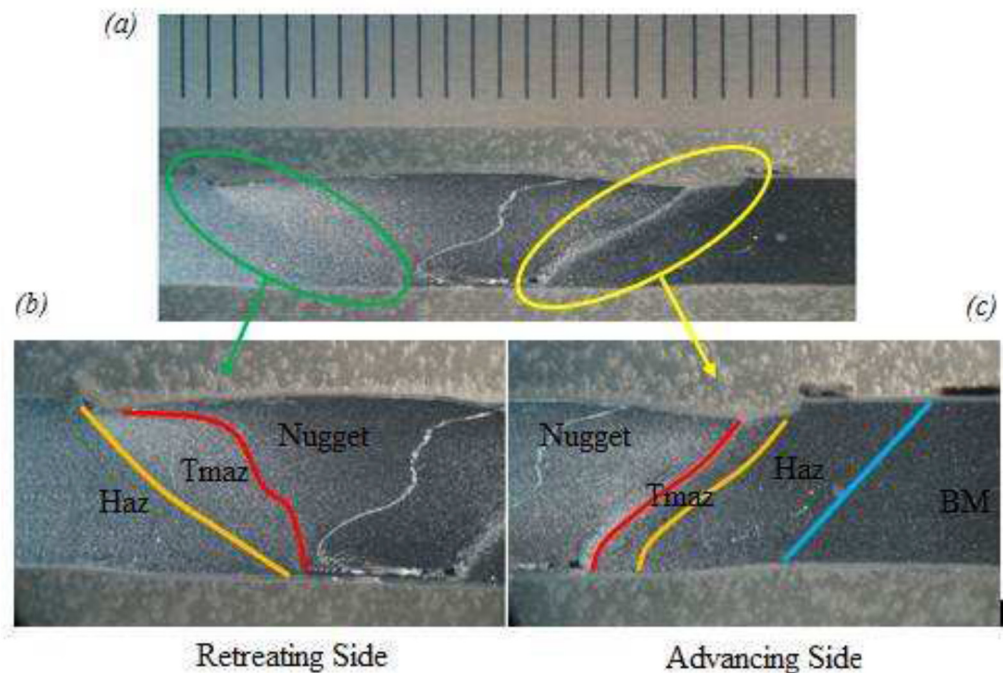


Figure 17. Macrograph of a friction stir-welded specimen, highlighting the important zones: (a) metallographic etching; (b) zoom of the retreating side (green zone in (a)); (c) zoom of the advancing side (yellow zone in (a)), reprinted with permission from [41], 2023, Trans Tech Publications.

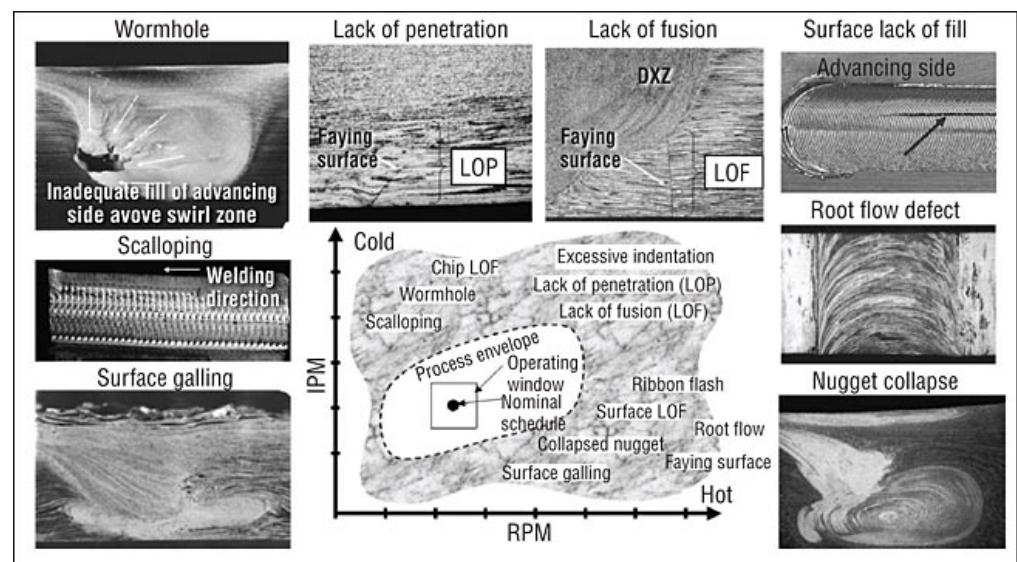


Figure 18. Most common defects as a function of the main process parameters, reprinted with permission from [83], 2023, Elsevier.

The necessity of performing a proper characterization as wide as possible is evident since defects such as tunneling and wormholes highly affect the mechanical properties of specimens yet are not visible at the surface. Typically, their occurrence is related to insufficient heat input [84] derived from a high advancing speed relative to the rotation speed; however, improper positioning of the tool may also contribute to their formation [76]. For instance, it has been reported that when performing OFSW/FSW on dissimilar materials,

the tool pin offset towards the weaker material prevents the formation of these tunneling defects, as depicted in Figure 19 [76].

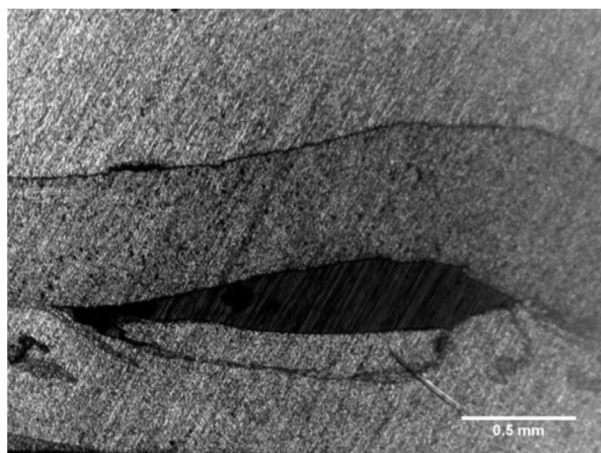


Figure 19. Tunneling defect, reprinted with permission from [76], 2023, Elsevier.

Furthermore, despite adopting a reasonable rotation-to-advancing speed ratio (not excessive cold or heat conditions), void defects and/or lack of fusion (commonly called a “kissing bond defect”) can also appear if the components of those velocities are excessively high for the tool used and/or the material to be joined due to abnormal stirring [84].

Other defects, such as a lack of penetration, are not directly related to the process parameters but instead are due to improper conditions in the system or apparatus. A simple way to avoid this defect lies in using a sacrificial anvil, allowing full penetration of the tool, and promoting a full joining of both parts without compromising the tool or the system. The sacrificial anvil can be a bottom plate of the same material for linear FSW or an internal pipe between the workpieces and inner mandrel when performing OFSW, followed by a grinding process until the desired thickness is achieved.

Even though the optimum parameters can be empirically achieved for a specific FSW application, i.e., for a specific type of joint, material, tool, geometry, and workpiece dimensions, it is not guaranteed that the same results of good surface finish, absence of defects, and mechanical properties are always obtained. Figure 20 shows a surface defect reported by Hatting et al. [22], and they stated that although the appropriate process parameters were maintained, a slight misalignment of the tool pin with the center of the joint, tube ovality, or eccentricity problems can be responsible for a poor-quality joint.



Figure 20. Surface defect observed by Hatting et al., reprinted with permission from [22], 2023, Elsevier.

3.8. Temperature Measurement and Profiles

As previously mentioned, one of the main advantages of FSW/OFSW/FSP over conventional fusion welding relies on its solid-state nature, avoiding the typical issues

and defects of the latter. Despite that, the temperature still presents a major impact on the weld quality and material properties of the FSW/OFSW process, as defects such as flash formation can occur if the attained temperature is too high, or defects such as wormholes tend to appear if the heat input is insufficient. There is a minimum heat, derived from not only the friction between the tool and workpiece, that is required to promote enough material softening to allow its solid-state mixture and achieve a consolidated weld. Note that the induced plastic deformation of the workpiece material also contributes to the temperature enhancement. It is commonly assumed that the tool shoulder is responsible for this heat generation, whereas the pin is accountable for the material stirring. According to the thermal model proposed by M. Selvaraj [85], the majority of the heat generated is indeed stemming from the shoulder (81%), while the influence of the pin accounts for the remaining 19% (16% deriving from the pin side and 3% deriving from the bottom of the pin). However, in favor of the process, achieving an optimal temperature for a unique weld, even if absent in the bibliography, can occur by varying the process parameters, i.e., by empirical methods. That is to say, if an increment in the heat input is required, it can be executed by diminishing the travel speed or enhancing the tool rotation speed. Note that, as quoted in the tool's chapter, certain tool features can be implemented that alter the material stirring or mixing and, consequently, adjust the heat input to the process.

It is commonly accepted that temperature is relevant to the process and weld quality; however, it seems that a consensus regarding the optimal temperature (relative to the alloy's solidus temperature, T_s) has yet to be reached. There is unanimity among most of the authors, though, that the required temperature does not exceed the alloy's melting point. However, some researchers claim that the material around the pin indeed achieves its solidus temperature, indicating local melting. If that is the case, the heat generation due to friction becomes a self-limiting system, tending to decrease since the material at the tool-workpiece interface shifts from a stick-to-slip phase. According to the literature, a temperature range between 60 and 90% T_s [86] can produce good-quality welds without defects, which is in agreement with what is observed in the orbital variant of the process. However, it seems there is consensus regarding the maximum temperature that the process can reach since the solidus temperature acts similar to a threshold, turning the process temperature into a self-regulated phenomenon. The phenomenon can be explained by shifting from a stick-slip phase at the tool-workpiece interface due to the local melting around the pin, reducing the generated heat due to friction, as previously stated. A temperature range of this magnitude can be assumed to be too wide, and there is a lack of unanimity as some authors claim that the weld temperature range required to produce sound welds is only a portion of this range [87]. In sum, one can conclude that even if the optimal welding parameters (and consequently the optimal temperature for a given alloy and geometry to be welded or processed) are not carried out, a good-quality weld free of defects can still be achieved. In other words, a sound weld should be attained for a range of process parameters instead of a defined set of those parameters. However, an optimization of the process is still recommended and can only be conducted empirically; despite some authors' claims of optimal parameters for a given alloy, they should vary according to the workpiece geometry, geometry, and features of the tool, and/or even the apparatus thermal flow.

Temperature measurement during FSW has been widely studied by various researchers adopting different methods, despite some uncertainties regarding the results attained. One of the main reasons for such uncertainty relies on the fact that temperature monitoring presents some difficulties, as such methods tend to be susceptible to measuring flaws. The most adopted methods are thermocouples embedded in the workpiece or the FSW tool, the use of a thermal camera, simulation models, and correlation with the observed microstructure evolution. Although less frequently used, temperature measurement methods based on ultrasound and neutron sources can also be selected. Despite the variety of methods, depicting the exact temperature of the different zones of the workpiece during the process presents some challenges since none of the above methods is without drawbacks.

Since the hottest point of the weld is claimed to be at the transition from the tool probe to the shoulder, the temperature measurement of the stir zone should be conducted as close as possible to that location. This can be a challenge when endorsing the use of thermocouples, which is the most common method, as their position in the workpiece is critical. Given the strong plastic deformation at the stir zone in addition to the probe rotation, the exact position of the thermocouple as the probe passes tends to be uncertain if it is located too close to the stir zone. If the thermocouples are positioned at the weld center, it has been reported that although they might not be destroyed by the probe passage, they may change their position due to the intense material flow, which will certainly alter the measurement accuracy [5]. In practice, just by using thermocouples, predicting the exact temperature in the joint line is impossible if they are positioned elsewhere due to the complex geometry, material tolerances, or clamping and backing components, which all influence the thermal flow during the process. Some studies have been conducted by using thermocouples embedded in the tool to perform online weld control; however, given the slow response of the probe thermocouple or the high disturbances observed in the thermocouple present in the tool shoulder, the results may not be precise. Furthermore, for small FSW tools, this technique requires a pre-drilled hole, increasing the cost of the process. Another limitation lies in the risk of thermocouple failure during the process due to the proximity of the tool-workpiece interface. However, it has been reported that the same embedded thermocouple has been used for over 7 m of successful welds without failure.

The tool-workpiece thermocouple (TWT) method, developed by Silva et al. [87], is another method to measure the temperature at the interface of the FSW tool and workpiece. It is based on the thermoelectric effect, where the weld temperature is related to the electric potential generated between the material of the tool and the workpiece material, as depicted in Figure 21. It should be noted that the obtained temperature values match the average temperature of the entire contact area, which can be a limiting factor depending on the study. Since the material properties (tool and workpiece) influence the temperature value, each tool-workpiece material combination requires a voltage-temperature relationship calibration. Despite these drawbacks, this method tends to be suitable for feedback control as well as use in the industrial environment.

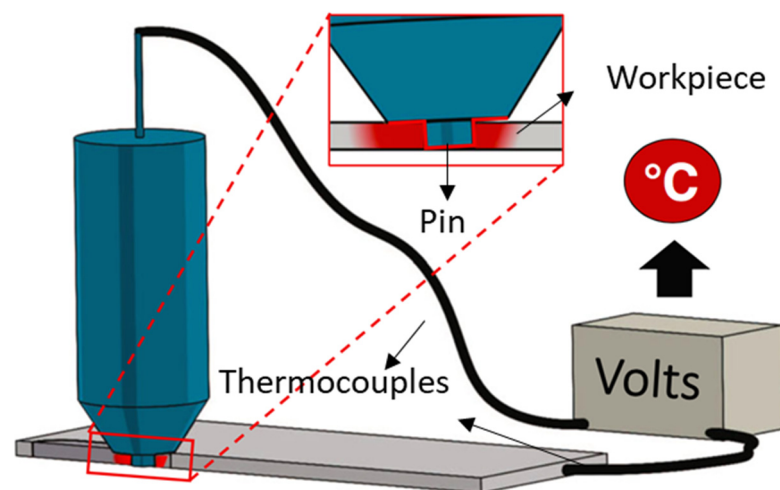


Figure 21. Tool-workpiece thermocouple (TWT) method used in FSW, reprinted with permission from [87], 2023, Springer Nature.

The use of thermal cameras has also gained some attention due to their simplicity of use during the process; however, their repeatability is compromised by other possible radiation sources. Furthermore, when using aluminum as a workpiece material, measurements are difficult due to its high reflectivity. To overcome this, the workpiece should be painted black in order to bring its emissivity closer to a value of one (~ 0.95).

Since it is known that temperature has a major impact on the observed microstructure of the workpiece, particularly in grain size, grain boundary, coarsening, and dissolution of precipitates, a relation between temperature estimation and the observed results can be established. However, this method does not simply give the exact temperature of the process; instead, one can report if a certain temperature threshold was achieved or not.

Numerical models, such as [75,85,88], among many others, have significantly contributed over the years to the research and knowledge about FSW, predicting material flow and residual stresses during the process, as well as attempting to predict energy input, efficiency, peak temperature, and thermal field. However, regarding these later thermal models, their flawless accuracy has yet to be confirmed because, to verify those models, accurate data is necessary and hard to obtain. The amount of acquired temperature data is insufficient to promote the valid spatial and temporal resolution that is required as input for the models, or even oversimplifications regarding uncertain variables, such as the thermal contact conductance between the workpiece and backing plate (mandrel in the OFSW case) or any other “path” of thermal flow [86,87].

Despite thermocouples being the most common method for temperature measurements of the FSW process, the obtained results are propitious misleads due to their high sensitivity regarding their location, so, if possible, complementary data should be acquired by selecting other methods, such as thermographic equipment, numerical models, the relation between temperature and the microstructure evolution, and/or the TWT method. If only one method of temperature control can be adopted, it should always be interpreted with caution, as none of the above is without faults, drawbacks, or difficulties.

Ismail et al. [39] conducted a study in order to acquire the characteristic temperature curves during the plunging stage (before the travel of the tool) of OFSW in an AA6063-T6 tubular specimen of 89 mm outside diameter and a thickness of 5 mm, carrying out a comparison between different tool rotational speeds from 900 to 1700 rpm. They maintained the other process parameters, such as a plunge depth of 4 mm, a plunge rate of 10 mm/min, an offset of 6 mm, and a dwell time of 30 s, and used K-type thermocouples to measure the temperature and position them as depicted in Figure 22. As expected, peak temperatures were achieved at the highest tool rotation speed (1700 rpm), and its temperature curve is presented in Figure 23, although it should be noted that the axial force was not measured and it is assumed that it was kept constant. Furthermore, across all the obtained results, the AS reached higher temperatures than the RS, varying from 5% to 25%. This phenomenon can be explained since the material deformation and flow are caused by the AS generating more heat from the plastic deformation when compared to the softer material left on the RS. Furthermore, higher frictional forces are achieved on the AS as the direction of the tangential component of the tool rotation and its transverse are the same, whereas in the RS those components are in opposite directions, generating less friction.

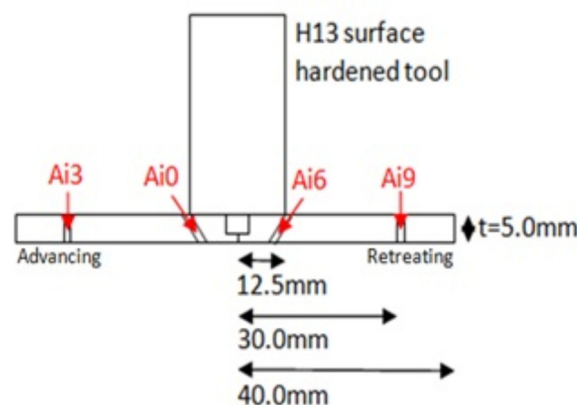


Figure 22. FSW process cross-section showing the thermocouple positioning, reprinted with permission from [39], 2023, Asian Research Publishing Network.

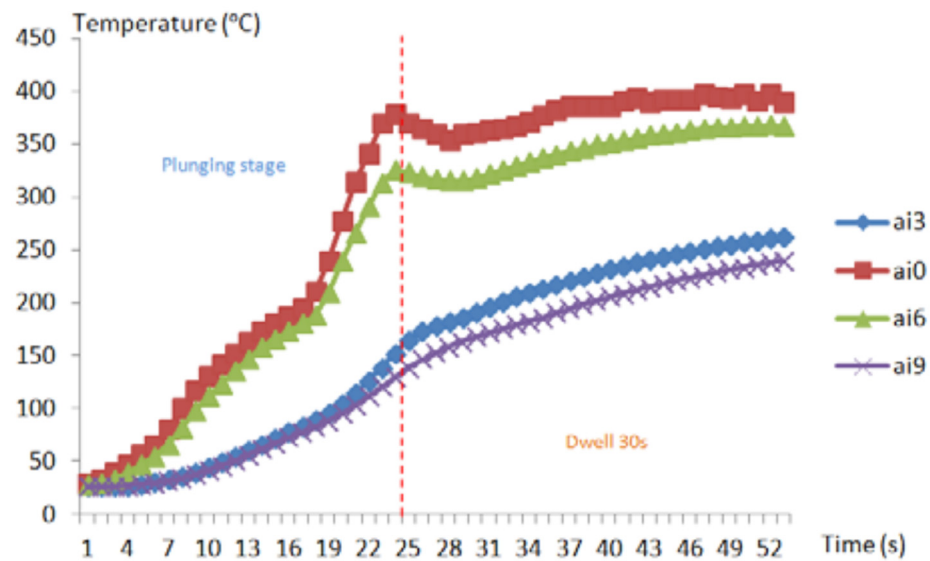


Figure 23. Measured temperatures for a 1700 rpm sample, reprinted with permission from [39], 2023, Asian Research Publishing Network.

A complete welding temperature history of an OFSW procedure for AA3003 and a pure copper dissimilar joint was recorded and analyzed by Chen et al. [40]. The small-diameter pipes (19 mm) had different thicknesses (1.5 mm and 1 mm for the Al pipe and the Cu one, respectively), and the results are depicted in Figure 24, using a tool rotation speed of 2400 rpm and a welding speed of 2 mm/s. The procedure consisted of a 400° workpiece rotation, meaning that the author performed a 40° rotation of an overlap region (OR), which is a requirement to mitigate the defects left at the beginning of the travel movement, followed by tool removal, and then re-inserted the pipes and performed a linear FSW in the direction of the x -axis, leaving the keyhole on the Al side. Since the objective of the work was only for research purposes, the solution seems valid; however, if industrial applications were intended, the authors should instead perform the linear part of the process by adopting a run-off ramp to leave the keyhole outside of the workpiece. By interpreting the peak temperatures, one can observe a rapid temperature increase during the plunge stage (~ 100 °C/s). As the travel movement started, a relatively stable increment (~ 3 °C/s) for the first OR passage was identified, following the same trend in the first region (FR) and middle region (MR), eventually reaching a plateau of ~ 260 °C at the workpiece rotation between 220° and 360° (last 140° for a complete rotation). In contrast, for the second passage in the OR, a decrease in temperature down to 220 °C is observed, which is related to the reduction in thickness promoted by the first welding passage. Given the obtained temperature history, the author identifies this variation in heat accumulation as an important feature of the OFSW process, particularly for small-diameter tubular specimens.

Cryogenic FSW is a variant of the process that has been successfully conducted by Benavides et al. [79] for linear FSW, with the temperature of the plates starting at -30 °C and not exceeding 140 °C. This variant of the process, although not published on OFSW yet, could be very appealing to materials that are heat- or age-treated, and it is necessary to maintain its properties since at these lower temperature issues such as the dissolution or heterogeneous distribution of precipitates should not occur. One attractive application for this variant could be an aerospace fuel tank, which will be subjected to high pressures, hence the high mechanical property requirements related to the aerospace industry.

3.9. Mechanical Properties

Mechanical testing is crucial to validating a good-quality weld. Indeed, one can assume a successful joining process by visual inspection of the surface finish or by resorting to metallographic analysis, where microstructural characterization is performed in addition

to defect identification if present. However, it is the mechanical testing that quantifies what is observed by metallography, concluding the viability of the process and the influence of the different microstructure zones, as well as the mechanical influence of those defects, if existent or detected. Since the process parameters have an impact on the microstructure of the specimens, it is expected that their mechanical properties are also dependent on those parameters, as has been studied and published regarding linear FSW [89].

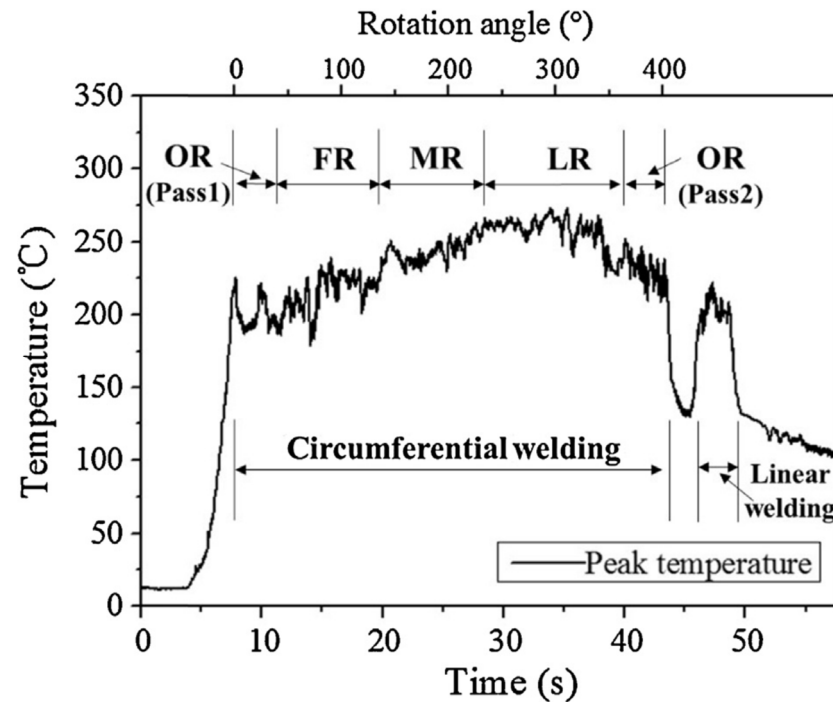


Figure 24. Temperature history of an OFSW procedure for AA3003 and a pure copper dissimilar joint, reprinted with permission from [40], 2023, Elsevier.

One highly important indicator of a good-quality weld is its tensile properties. The term “joint efficiency” is often used to evaluate the quality of the weld, which consists of the ratio between the tensile strength of the weld and the base material. Additionally, given the different zones typically observed by the optical microscope, microhardness profiles tend to be plentiful in published work since they are a way to complement and quantify the information obtained by microstructure analysis. Hence, most of the mechanical testing lies in these two characterization methods.

3.9.1. Weld Strength

Generally, conventional tensile testing is suitable to evaluate the mechanical properties of an FSW joint [42]; however, if tensile testing specimens are not possible to produce due to machining or dimension limitations, evaluation of tubular workpieces can be conducted instead by tube bulge testing for circumferential [44] and longitudinal welds [90], which has been reported as a valid method of mechanical characterization. As a rule, a good weld can be identified if its fracture during tensile testing does not occur in the nugget zone, meaning that it is not the weakest part of the specimen. However, this does not mean that the base material is the limiting factor; indeed, it is not, since, as mentioned in the microstructure section, the HAZ is categorized as the zone with the lowest strength due to grain coalescence and coarsened precipitates. When applying tension during testing, this is the zone where most of the strain occurs (12–14%), whereas in the nugget zone, the resulting strain tends to be 2–5%. As a consequence of the higher strain intrinsic in the HAZ, necking followed by fracture occurs in this zone if a good-quality weld is achieved [5]. Furthermore, it has been reported that the fracture should occur at the RS given the different intrinsic strength and ductility of both sides and the RS’s lower strength.

Hattingh et al. [22] performed OFSW in AA6082-T6 tubes, and during tensile testing, although failure occurred consistently in the RS of the tool, the location of the fracture was in the welding zone for the micro-tensile specimens. However, when conducting the tensile testing for the tubular specimens instead, failure occurred on either AS or RS at the shoulder undercut, which is explained by being an area of stress concentration and carrying a lower load.

Tensile testing specimens cut from tubular workpieces joined by OFSW are depicted in Figures 25 and 26, with outer diameters of 40 mm and 19 mm, respectively. A more detailed table regarding the obtained mechanical testing results of other OFSW published work is presented in the following Summary sub-chapter as a way to compare not only different materials but also what the authors claim as the best process parameters, i.e., the process parameters from which the highest joint efficiency was achieved. Since the focus of this review article lies on the orbital variant of friction stir welding, the analysis of the mechanical characterization will not be too meticulous due to the similarities with linear FSW or even with any processing technology, which are widely explained in the literature. However, emphasis should be given to the work of Chen et al. [40] since it distinguishes itself among the other works not only due to the dissimilar material nature of the joint but also due to the relatively small workpiece outer diameter (19 mm) from which four tensile testing specimens were cut. Those four specimens match four different stages of the process, and their abbreviations, shown in Figure 26, are FR, MR, LR, and OR, which stand for the former region, the middle region, the later region, and the overlap region, respectively. Figure 27a presents the obtained tensile testing results and macrographs relative to the fracture locations for each of the specimens. Due to the dissimilar nature of the specimens (Al 3003–Cu joint), it is expected that if a proper weld is achieved, the fracture location should be at the weaker side, in this case at the HAZ of the Al side, which is verified for the LR specimen. However, the remaining specimens have experienced a brittle fracture in the nugget region propagated along or perpendicular to the band structures of the nugget close to the Al/Cu interface. Nonetheless, it should be noted that the thickness of the samples is not constant, meaning that the area also differs from specimen to specimen, which directly influences the obtained strength (MPa). So, despite the LR specimen reaching a tensile force of 1191 N (for an area of 6.87 mm²), the OR sample exhibited the highest strength (213 MPa) due to the inferior area. The author explains the ductile fracture of the LR sample since it was in this region that a stable and peak process temperature was achieved (~260 °C), as depicted in Figure 24 in the “Temperature Measurement and Profiles” section.

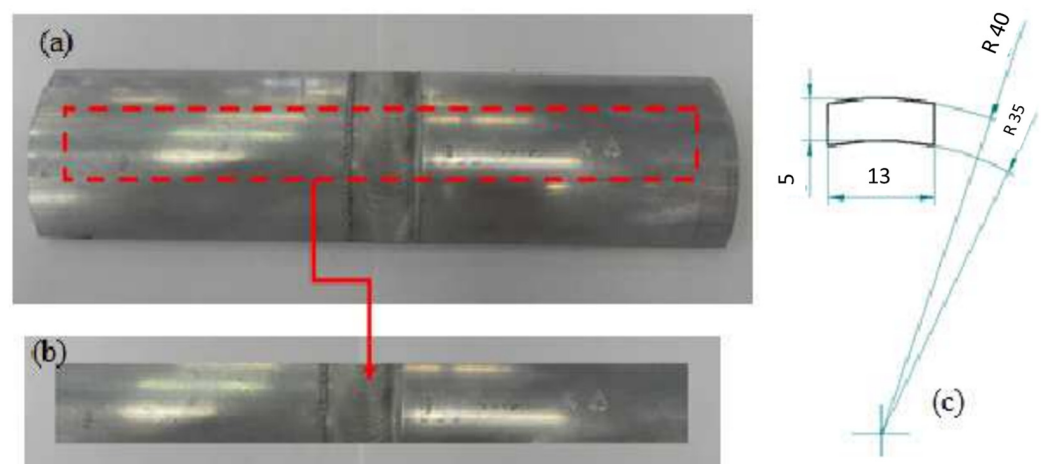


Figure 25. Tensile testing specimens cut from 40 mm tubular workpieces joined by OFSW: (a) part realized with the process in regime condition; (b) specimen for the tensile test; (c) measures of the specimen, reprinted with permission from [42], 2023, Trans Tech Publications.

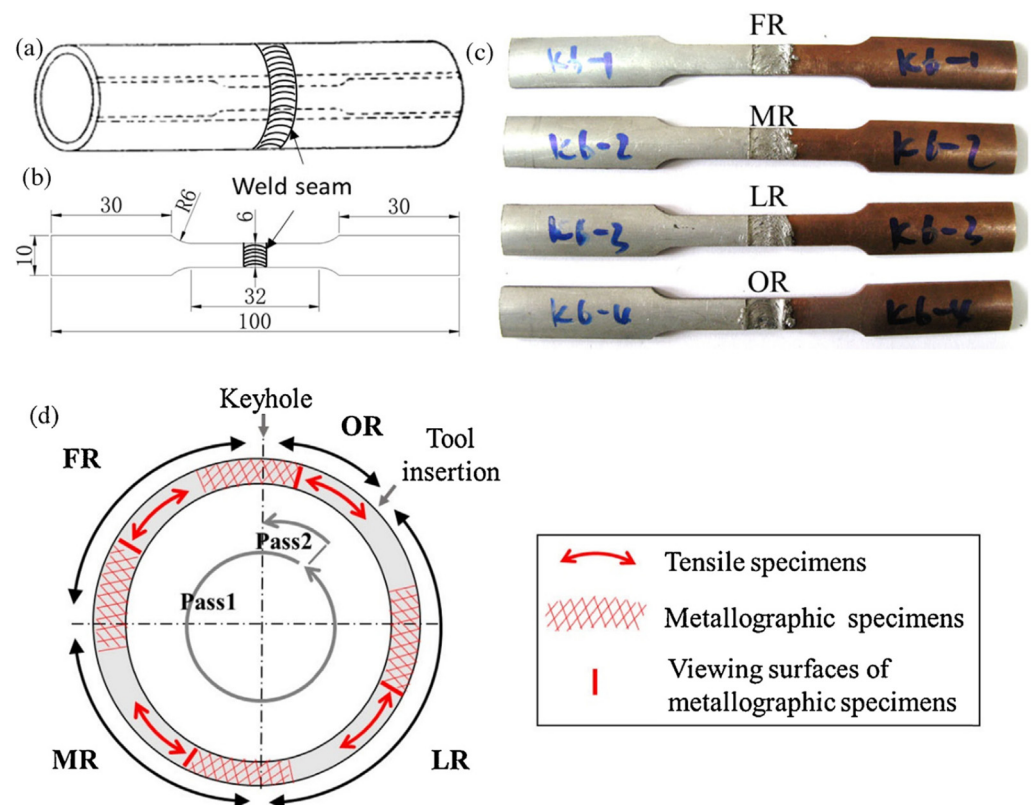


Figure 26. Extract locations of specimens on a 19 mm tubular OFSW workpiece joint: (a) schematic diagram showing how the tensile specimens were cut from the joint; (b) dimensions of the tensile specimens (in mm); (c) tensile specimens; (d) schematic diagram of the weld region, reprinted with permission from [40], 2023, Elsevier.

Aliha et al. [91] intended to evaluate the fracture toughness by performing 3-point bending testing as a complement to tensile testing on a non-treated AA6063 alloy tube in both the transverse (T) and longitudinal (L) directions on OFSW and BM samples, as depicted in Figure 28. Note that the fracture location was premeditated since all samples were pre-cut by a wire-cut machine. Those cuts were located at the center of the samples on the opposite side of the 3-point bending fixture's middle rolling support (where tension occurs instead of compression), and their length was 0.5 of the "thickness" to be tested ($a = \frac{t}{2}$ and $a = \frac{w}{2}$ for the T-direction and L-direction, respectively). The test was performed with a fixed loading span ratio (S/L) of 0.8, and the samples were loaded at a constant rate of 1 mm/min until failure in all specimens, with the results presented in Figure 29. By observing the curves obtained, several conclusions can be drawn. Firstly, although not related to the OFSW process, just by comparing both T and L directions, it is evident that both fracture load and fracture energy values of the T-direction samples were superior to the L-direction ones, whereas the samples of the L-direction revealed a slightly superior ductility, despite all fractures being classified as ductile instead of brittle. This is due to the anisotropic nature of tubular specimens if they are not annealed. Then, the influence of the OFSW process stands out since the fracture energy values achieved were two times greater than those achieved for the BM samples. Note that, as the formation of smaller and finer grains occurs in the SZ, the load-bearing capacity of the material should increase, as verified in the load-displacement curve, since both the crack growth resistance and the maximum peak carrying load before breaking were improved by the process in both directions. Furthermore, the loading required to promote plastic deformation was also greatly improved by the process in both directions, although more significantly in the T-direction samples. Lastly, only the displacement in which fracture occurred was reduced by the process, revealing that the process, in this case, decreased the material's ductility

in comparison with the BM samples. In sum, not only is OFSW a viable solution for successfully joining materials, but also OFSP can present great improvements in the material mechanical properties of non-heat-treated aluminum alloys.

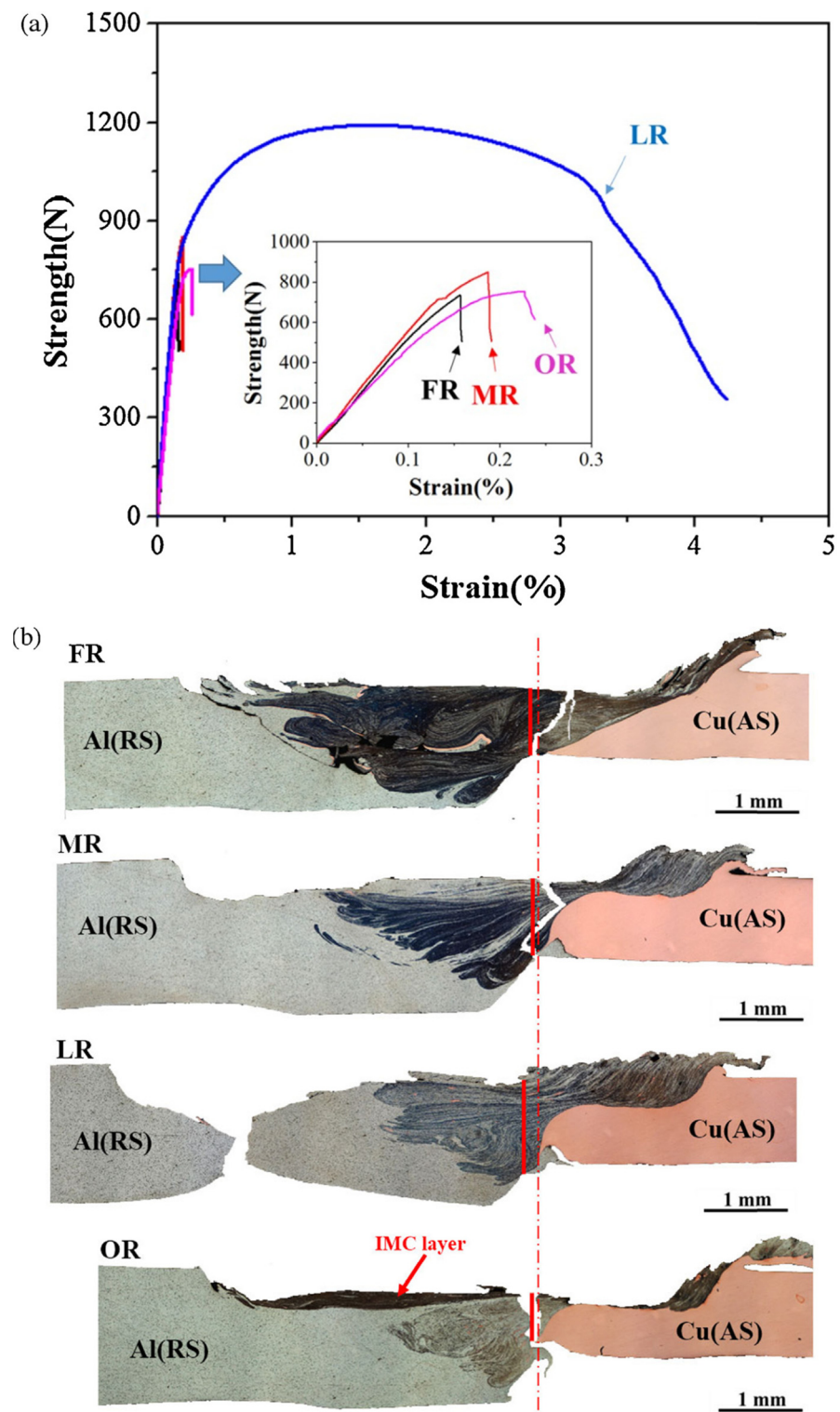


Figure 27. (a) Obtained tensile testing results and (b) macrographs relative to the fracture locations for the specimens, reprinted with permission from [40], 2023, Elsevier.

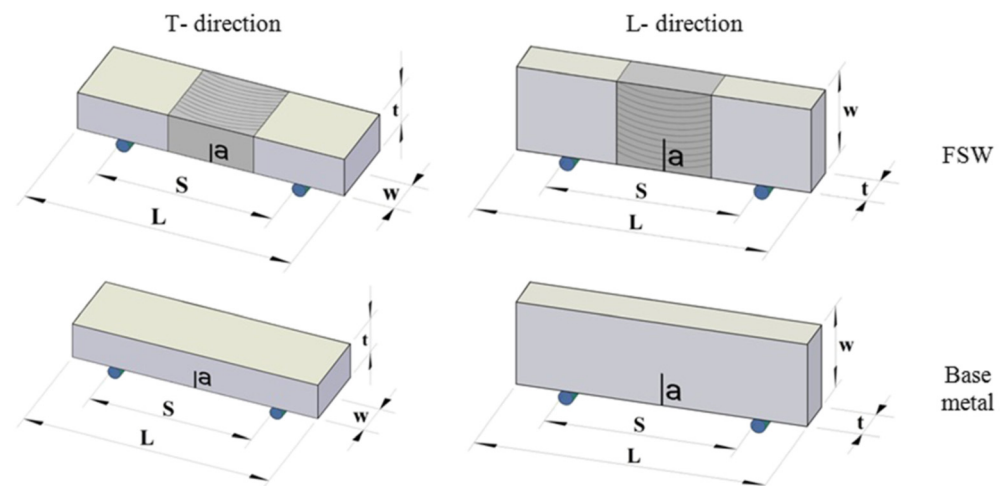


Figure 28. Schematic illustration of fracture toughness specimens, with permission from [91], 2023, John Wiley and Sons.

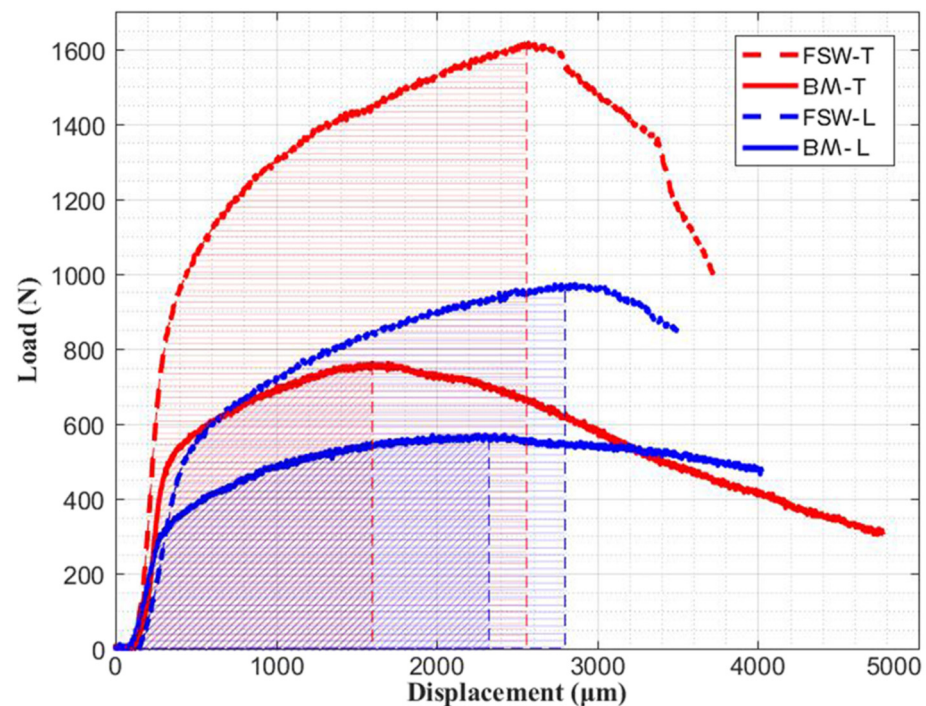


Figure 29. Fracture toughness curves for a 3-point bending test, with permission from [91], 2023, John Wiley and Sons.

3.9.2. Microhardness

Across the literature, microhardness testing is the most widely adopted characterization of the specimens' mechanical properties. Despite requiring some preparation of the samples, such as cutting, grinding, and polishing, this testing method is relatively easy to perform, given the information that can be acquired from those microhardness profiles as a complement to what is observed and identified as characteristic zones by macro and microstructural characterization.

When determining the influence of the FSW/OFSW process on the hardness of the material, a distinction between heat-treatable (precipitation-hardenable) alloys and non-heat-treatable (solid-solution-hardened) alloys is often emphasized in aluminum alloys; however, a more noticeable variation in the hardness profiles is evident when performing FSW/OFSW in annealed alloys, as great improvements can be achieved in comparison

with the base material. Two hardness profiles obtained from OFSW-produced specimens of the same material (AA5456) but different temper conditions (AA5456-O (annealed) and AA5456-H321 (strain-hardened)) are presented in Figure 30, where the process parameters, as well as the tool, were maintained [36]. Furthermore, each microstructure zone is easily identified and distinguished from the others by the variation of hardness values across the profiles. Regarding the strain-hardened specimen, a typical “W”-shaped microhardness is observed, whereas none of the identified zones matched the BM hardness values, despite the SZ’s values coming close. Despite benefiting from grain refinement in addition to the recrystallization of finer and equiaxed grains, which tend to enhance the material’s hardness, the influence of dissolution and coarsening of strengthening precipitates in addition to the decrease in density of dislocations is enough to decrease the hardness values in the SZ relative to the base material. In contrast, regarding the annealed specimen, a clear improvement is observed (> 10%), particularly in the SZ, as the author justifies this enhancement by grain size strengthening as well as dislocation looping effects at the center of the weld, which can be useful for not only OFSW but also OFSP in these annealed alloys. Moreover, the profile shape regarding the HAZ and TMAZ regions is similar in both samples, decreasing from the BM and eventually achieving the minimum value in the advancing side of HAZ and then increasing up the SZ values in the TMAZ, where a peak is observed at the AS, as explained by the distinctive grain boundaries on this side. The author explains the inferior values attained in the AS of HAZ, given the higher heat generation at the AS due to material shearing or deformation rather than predominant material flow at the RS. When performing OFSW under various parameters, the author also verified the inverse relation between the tool rotation speed and the correspondent microhardness values, since higher rotation speeds promote higher heat inputs, which will favor grain coarsening or growth that, according to the Halls-Patch relationship, will negatively impact the hardness values. Similar results were confirmed by Aval et al. [37], who performed an AA5083-H321/AA5083-O OFSLW procedure under different parameters (Figure 31c). By just varying the tool rotation speed while maintaining the other parameters, the microhardness profiles revealed that not only did the sample obtained using the higher tool rotation speed (sample C—800 rpm) achieve lower microhardness results relative to the one obtained by the lower tool rotation speed (sample B—650 rpm), but also the width of the HAZ was influenced by this increase in heat input, as depicted in Figure 31a,b. The same conclusion was also supported by D’Urso et al. [42] when performing OFSW on a heat-treated AA6063-T6 since higher HAZ width on those profiles was attained by decreasing the welding speed or by increasing the tool rotation speed while the tool and other process parameters were kept constant. Being a heat-treated alloy, none of the microstructural zones revealed microhardness values superior to or equal to the BM, as expected. However, in that work, the minimum microhardness was consistently identified on the RS instead of the AS, despite being relatively similar. Nonetheless, more contradictory results have been published, such as the work conducted by Aliha et al. [91], who performed OFSW on AA6063 alloy, where, although the average hardness at the weld center improved when compared to the base material, which can be useful to process these non-heat-treated alloys in addition to welding, the author claims higher hardness values were attained by decreasing the welding speed (i.e., by increasing the heat input during the process). Such differences regarding the microhardness distribution can be explained by the work conducted by Kumar et al. [45], who performed a double-sided OFSW on X80-grade steel pipes, where the parameters of the process were kept constant except for the tool. Two tools were adopted, one made of PCBN and the other of W-Re. In addition to the different materials, the tools also exhibited different geometries, as the PCBN tool consisted of a more traditional tool design with a noticeable shoulder and pin, and the W-Re tool consisted of a tapered pin with a small shoulder relative to the pin’s diameter. Despite the microhardness values being of the same magnitude, their distribution on the maps is different. While the microhardness map obtained from the PCBN tool revealed an asymmetric (about at the centerline of the weld) swirl-like pattern distribution with higher values on the advancing

side, the map derived from the W-Re tool exhibited a relatively symmetrical distribution about the center of the weld. The author concludes that such discrepancy is explained by the geometry of the tool, as it has a significant influence on localized microhardness derived from the differences in thermo-mechanical histories of the SZ, i.e., the material flow patterns around the tool.

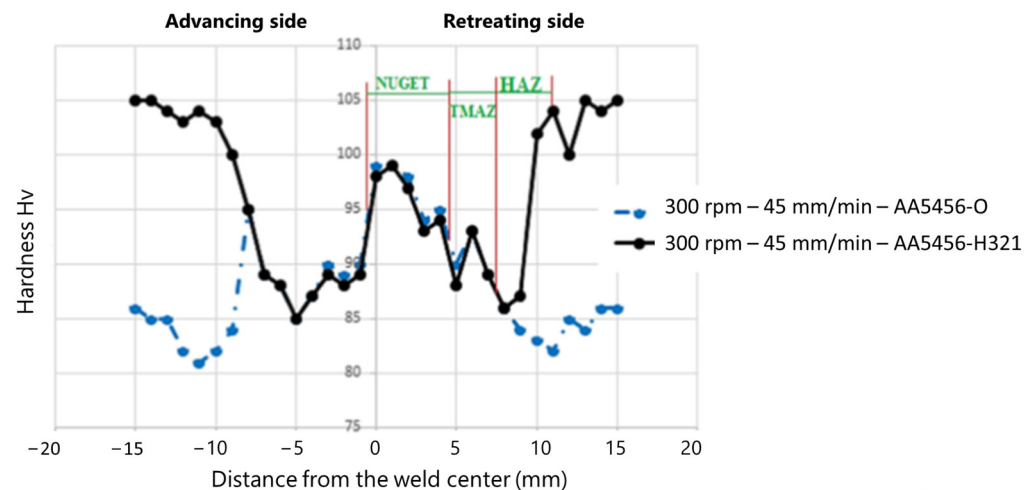


Figure 30. Microhardness profile across a welded joint obtained at 300 rpm and 45 mm/min, reprinted with permission from [36], 2023, Springer Nature.

In sum, despite the microhardness values being somewhat estimated depending on the alloy's heat treatment, their exact distribution highly depends on the type of tool used during the process in addition to the workpiece material and the remaining process parameters.

3.9.3. Summary

This sub-chapter contains a comparison table (Table 4) that is composed of the obtained results regarding mechanical testing of OFSW-produced specimens, namely the joint efficiency, microstructure zones where maximum and minimum hardness were attained, as well as their quantification and comparison with the base material's value and the best operating parameters, particularly the tool rotation speed and welding speed. It should be noted that, in the majority of the published work, this "best operating parameters" section is related to the highest joint efficiency; however, some authors did not perform any tensile testing and concluded best parameters based on specimens with no defects, higher hardness or microhardness values, homogeneity, or even workpiece surface appearance. Given the variety of materials and tools selected, in addition to the unique specimen geometries and dimensions and the limited mechanical characterization, comparing the claimed best parameters should not be viable, not only because there is a limitation to the sets of parameters that have been tested but also due to the vastly unique initial and process conditions of each work. In sum, when authors refer to "the best parameters," it should not be generalized by material, tool, or any other isolated condition but instead by a combination of them all, i.e., the best operating parameters are obtained from what has been tested under specific working conditions. This does not repeal the usefulness of this data, as it can serve as a guide for future work, narrowing the process parameter range before performing OFSW. However, the optimization itself should be conducted empirically for a given application.

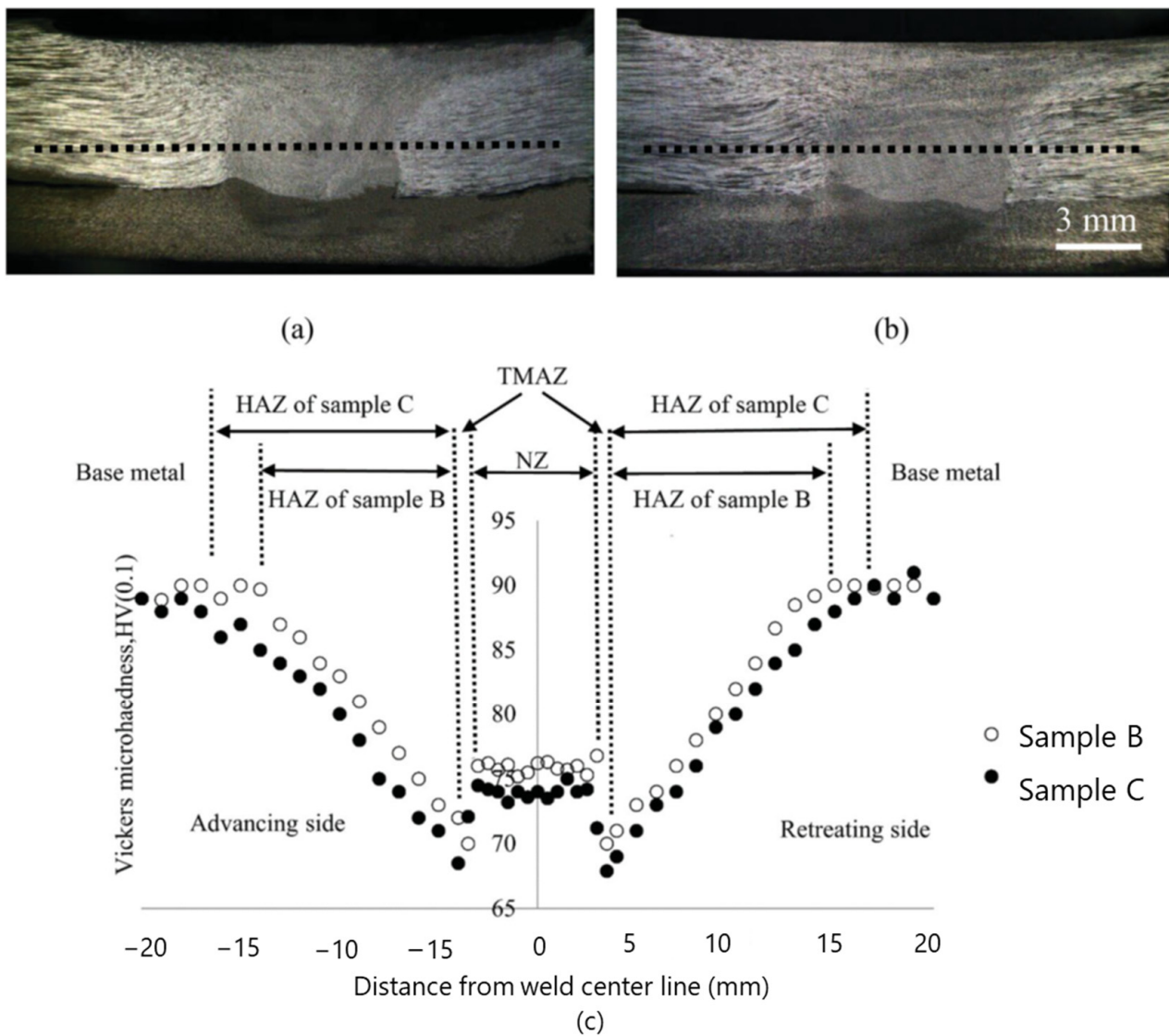


Figure 31. Macrostructure of the lap joint and the microhardness test line of (a) sample B and (b) sample C. (c) Microhardness distributions at the AA5083-H321 part of samples B and C, reprinted with permission from [37], 2023, Taylor & Francis.

Table 4. Comparison table regarding base material, parameters, and mechanical performance.

Workpiece Material	Type of Joint	Best Operating Parameters	Base Material Hardness	Maximum Hardness (zone)	Minimum Hardness (zone)	Joint Efficiency	Reference
AA5456-O (2.5 mm thickness) AA5456-H321 (5 mm thickness) D: 370 mm	OFSW (lap joint)	900 rev·min ⁻¹ 45 mm/min	84 HV (AA5456-O) 104 HV (AA5456-H321)	98 HV (SZ, AA5456-H321) 98 HV (SZ, AA5456-O)	85 HV (AS of HAZ, AA5456-H321)	303 MPa (dissimilar weld) 5456-H321(386 MPa) 5456-O (326 MPa) 79–93%	[36]
AA5083-H321 (5 mm) AA5083-O (2.5 mm) D: 360 mm	OFSW	650 rpm 40 mm/min (Sample B)	92 HV (AA5083-H321) 85 HV (AA5083-O)	73 HV (SZ, AA5456-H321 76 HV (SZ, AA5456-H321, Sample B)	66 HV (HAZ. AA5456-H321)	AA5083-H321 (316 MPa) AA5083-O (293 MPa)	[37]
AA6063 (5 mm) D: 89 mm	OFSW (butt joint)	1500 rpm 1.8 mm/s	Does not specify the temper (AA6063-T6?)	37.5 HRB (converter for HV) (travel speed 1.8 mm/s)	35 HRB (converter for HV) (SZ) (900 rpm)		[38]
AA6063-T6 (5 mm) D: 89 mm	OFSW						[39]
AA6061-T6 (5.1 mm) D: 107 mm	OFSW	15.7 rpm (400 mm/min) 1600 rpm	107 HV	-	-	70%	[32]
AA3003 (1.5 mm) Pure Cu (1 mm) OD: 19 mm	OFSW					89%	[40]
AA6061-T6	OFSW	630 rev·min ⁻¹ 1 mm/s	107 HV		HAZ	61.7%	[41]
AA6060-T6 (5 mm) D: 80 mm	OFSW	1000 rev·min ⁻¹ 200 mm/min	77–83 HV			111.3 MPa 189 MPa 59%	[42]
AA6063-T6 (5 mm) D: 100 mm	OFSW	710 rpm 2.87 mm/s					[43]
AA 2024-O (5 mm)	Spiral Weld					266 MPa 234 MPa 114 %	[44]
AA6082-T6 (3.5 mm) OD: 38 mm	OFSW	600 rpm 100 mm/min				169 MPa 303 MPa 56 %	[22]

Table 4. Cont.

Workpiece Material	Type of Joint	Best Operating Parameters	Base Material Hardness	Maximum Hardness (zone)	Minimum Hardness (zone)	Joint Efficiency	Reference
Commercial Pipeline Steels X65–X120 (16–19 mm) D: 762 mm	OFSW Two-sided welds (11–12 mm each)		270 HV	310 HV (SZ)	190–210 HV (Overlap)	712 MPa 659 MPa 108%	[45]
AA6063	OFSW					84.2 %	[46]
API Grade X65, X80, X100, and L80 Steels (13 mm) ID: 305 mm	OFSW	-	-	-	-	-	[17]
AA6061							[47]
X42 Carbon Steel (12 mm) OD: 320 mm	OFSW						[26]
AA6063 (10 mm) OD: 140 mm	OFSW	800 rpm 120 mm/min	46	65 (SZ) 1000 rpm, 45 mm/min	28 (HAZ) 1250 rpm, 120 mm/min	98.5 %	[90]

4. Future Perspectives and Trends

Despite being around for over 30 years, the FSW technology is still considered relatively young, and great improvements could be made in future years regarding various aspects of the process. Furthermore, new improvements are expected given the present and continuous advances in robotics and automation, as well as in metal additive manufacturing. Some current trends in FSW include material diversity (including magnesium and copper alloys), process optimization (to increase efficiency and quality and reduce costs), application expansion (in the shipbuilding and aerospace industries), automation, and hybrid processes (when FSW is combined with other welding techniques, such as laser welding).

Therefore, the orbital variant of the FSW process should not be limited to just “orbital” movements but instead any curvilinear path, not only as a welding technology but also as a processing one that benefits from the possibility of application to workpieces with more complex geometries. Such material processing can be performed by the conventional FSP method by introducing structural and/or functional particles by different methods, such as upward friction stir processing (UFSP) [92], or even by incorporating distinct features, such as friction stir-based channeling. As reported by the TWI, friction stir-based channeling was revealed to be remarkably promising in orbital applications, such as relatively compact-size heat exchangers for different thermal management tubular systems, for instance, pipe cooling [93]. Likewise, trends in OFSW encompass better weld quality (attributed to enhanced material mixing and increased tool life), the ability to join complex geometries, improved productivity, and process optimization, including tool design and rotational speed, among others.

Regarding the FSW/OFSW process, as the understanding of all the technological phenomena expands, the trend should continue in the direction of improving the tools. Such improvement can be attained by adopting or developing new tool materials, aiming to achieve a wider range of materials to be joined or processed in addition to increasing the tool’s life cycle, which is a current limiting factor, particularly in higher-strength materials, and lowering processing costs over time. Simultaneously, another way to upgrade tools should be through innovation of different tool geometries and features, given that material flow insight and simulations are becoming more precise, as a means of turning the process as low-force-demanding and cold as possible, therefore amplifying the use of FSW/OFSW in different industrial applications. Consequently, as the inherent forces and equipment stiffness demand trends diminish due to the tool’s optimization, smaller, portable, and more versatile equipment should become more commercially available, enabling the process to be performed on-site, which is, at present, a decisive constraint for considerable industrial applications.

Author Contributions: F.B.F.: writing—original draft preparation, formal analysis, investigation. I.F.: formal analysis, investigation, writing—review and editing; I.B.: formal analysis, investigation, J.P.O.: writing—review and editing, supervision; T.S.: writing—review and editing, funding acquisition, supervision. All authors have read and agreed to the published version of the manuscript.

Funding: The authors acknowledge the Portuguese Agência Nacional de Inovação (ANI), through the project SI I&DT (PROJETOS MOBILIZADORES), N° 024534-“INFANTE-Microsatélite para Vigilância Marítima, Observação da Terra e IoT no contexto de constelações”, co-financed by PORTUGAL2020, through Fundo Europeu de Desenvolvimento Regional (FEDER).

Data Availability Statement: Not applicable.

Acknowledgments: The authors acknowledge the Portuguese Agência Nacional de Inovação (ANI), through the project SI I&DT (PROJETOS MOBILIZADORES), N° 024534-“INFANTE-Microsatélite para Vigilância Marítima, Observação da Terra e IoT no contexto de constelações”, co-financed by PORTUGAL2020, through Fundo Europeu de Desenvolvimento Regional (FEDER). Authors acknowledge the Portuguese Fundação para a Ciência e a Tecnologia (FCT-MCTES) for its financial support via the project UID/EMS/00667/2019 (UNIDEMI). Authors acknowledge funding by national funds from FCT-Fundação para a Ciência e a Tecnologia, I.P., in the scope of the projects LA/P/0037/2020,

UIDP/50025/2020 and UIDB/50025/2020 of the Associate Laboratory Institute of Nanostructures, Nanomodelling and Nanofabrication–i3N.

Conflicts of Interest: The authors declare no conflict of interest.

References

1. Thomas, W.M. Friction Stir Butt Welding. International Patent Application PCT/GB92, Patent Application GB9125978.8, 6 December 1991.
2. Ding, R.J.; Carter, R.W. Orbital Friction Stir Weld System. U.S. Patent APPL-SN-216484, 10 July 2001.
3. Peterson, S.M.; Hall, J.; Steel, J.; Babb, R.J.; Collier, J.; Packer, M. Out of Position Friction Stir Welding of Casing and Small Diameter Tubing or Pipe. WIPO WO2011/053361 A3, 5 May 2011.
4. Rams, B.; Pietras, A.; Mroczka, K. Friction Stir Welding of Elements Made of Cast Aluminium Alloys. *Arch. Metall. Mater.* **2014**, *59*, 385–392. [\[CrossRef\]](#)
5. Mishra, R.S.; Ma, Z.Y. Friction stir welding and processing. *Mater. Sci. Eng. R Rep.* **2005**, *50*, 1–78. [\[CrossRef\]](#)
6. Rohrberg, R.G.; Stanley, A.E. Welding Apparatus. U.S. Patent 3,238,347, 1 March 1966.
7. de Garcia, J.A.O.; de Lima, G.L.; Pereira, W.D.B.; Guimarães, V.A.; de Moura Neto, C.; Paranhos, R.P.R. Characterization of titanium welded joints by the orbital gas tungsten arc welding process for aerospace application. *J. Aerosp. Technol. Manag.* **2010**, *2*, 211–218.
8. Ayof, M.N.; Hussein, N.I.S.; Noh, M.Z.M. Gas Metal Arc Welding Parameters Effect on Properties of Tailored Orbital Weld of SS304 and BS1387. *IOP Conf. Ser. Mater. Sci. Eng.* **2017**, *238*, 12–15.
9. United States Automotive Materials Partnership. United States Automotive Materials Partnership LLC (USAMP). United States; 31 January 2011. Available online: <https://www.osti.gov/biblio/1038533> (accessed on 21 May 2023).
10. Ai, Y.; Yu, L.; Huang, Y.; Liu, X. The investigation of molten pool dynamic behaviors during the “∞” shaped oscillating laser welding of aluminum alloy. *Int. J. Therm. Sci.* **2022**, *173*, 107350. [\[CrossRef\]](#)
11. Ai, Y.; Liu, X.; Huang, Y.; Yu, L. Numerical analysis of the influence of molten pool instability on the weld formation during the high speed fiber laser welding. *Int. J. Heat Mass Transf.* **2020**, *160*, 120103. [\[CrossRef\]](#)
12. Baek, D.; Moon, H.S.; Park, S.H. Development of an automatic orbital welding system with robust weaving width control and a seam-tracking function for narrow grooves. *Int. J. Adv. Manuf. Technol.* **2017**, *93*, 767–777.
13. Górka, J.; Przybyła, M.; Szmul, M.; Chudzio, A.; Ładak, D. Orbital TIG Welding of Titanium Tubes with Perforated Bottom Made of Titanium-Clad Steel. *Adv. Mater. Sci.* **2019**, *19*, 55–64. [\[CrossRef\]](#)
14. Gomes, J.F.; Miranda, R.; Santos, T.J.; Carvalho, P. Emission of nanoparticles during friction stir welding (FSW) of aluminium alloys. *J. Toxicol. Environ. Heal.-Part A Curr.* **2014**, *77*, 924–930. [\[CrossRef\]](#)
15. Engelhard, G.; Hillers, T.; Pellkofer, D. Orbital Friction Stir Welding of Aluminium Pipes. In Proceedings of the TWI 3rd International Symposium on Friction Stir Welding, Kobe, Japan, 27–28 September 2001.
16. Riffel, K.C.; Silva, R.H.G.; Dalpiaz, G.; Marques, C.; Schwedersky, M.B. Keyhole GTAW with Dynamic Wire Feeding Applied to Orbital Welding of 304L SS Pipes. *Soldag. Insp.* **2019**, *24*, 1–11. [\[CrossRef\]](#)
17. Defalco, J.; Steel, R. Friction Stir Process Now Welds Steel Pipe. *Weld. J.* **2009**, *88*, 44–48.
18. Carter, B. Introduction to Friction Stir Welding (FSW). Available online: <https://ntrs.nasa.gov/api/citations/20150009520/downloads/20150009520.pdf> (accessed on 21 May 2023).
19. Callister, W.D.; Rethwisch, D.G. *Materials Science and Engineering: An Introduction*; Wiley: New York, NY, USA, 2020; Volume 7.
20. Rai, R.; De, A.; Bhadeshia, H.K.D.H.; DebRoy, T. Review: Friction stir welding tools. *Sci. Technol. Weld. Join.* **2011**, *16*, 325–342. [\[CrossRef\]](#)
21. Zhang, Y.N.; Cao, X.; Larose, S.; Wanjara, P. Review of tools for friction stir welding and processing. *Can. Met. Q.* **2012**, *51*, 250–261. [\[CrossRef\]](#)
22. Hattingh, D.; von Welligh, L.; Bernard, D.; Susmel, L.; Tovo, R.; James, M. Semiautomatic friction stir welding of 38 mm OD 6082-T6 aluminium tubes. *J. Mater. Process. Technol.* **2016**, *238*, 255–266. [\[CrossRef\]](#)
23. Hilgert, J.; Dos Santos, J.F.; Huber, N. Shear layer modelling for bobbin tool friction stir welding. *Sci. Technol. Weld. Join.* **2012**, *17*, 454–459. [\[CrossRef\]](#)
24. Dialami, N.; Cervera, M.; Chiumenti, M. Effect of the tool tilt angle on the heat generation and the material flow in friction stir welding. *Metals* **2019**, *9*, 28. [\[CrossRef\]](#)
25. Ding, R.J.; Oelgoetz, P.A. Auto-Adjustable Pin Tool for Friction Stir Welding. US5893507, 13 April 1999.
26. Mahoney, M.; Sanderson, S.; Feng, Z.; Steel, R.; Packer, S.; Fleck, D. Friction Stir Welding of Pipeline Steels. In *Friction Stir Welding and Processing VII*; Mishra, R., Mahoney, M.W., Sato, Y., Hovanski, Y., Verma, R., Eds.; Springer International Publishing: Cham, Switzerland, 2016; pp. 59–69.
27. Kishore prasaath, K.; Manikandan, T.; Shanmugapraveen, S.; Ponnmurugan, M. Friction Stir Welding in Circular Pipes. *Int. Res. J. Eng. Technol.* **2018**, *5*, 664–666.
28. DebRoy, T.; De, A.; Bhadeshia, H.K.D.H.; Manvatkar, V.D.; Arora, A. Tool durability maps for friction stir welding of an aluminium alloy. *Proc. R. Soc. A Math. Phys. Eng. Sci.* **2012**, *468*, 3552–3570. [\[CrossRef\]](#)

29. Reynolds, A.P.; Tang, W. Alloy, tool geometry, and process parameter effects on friction stir weld energies and resultant FSW joint properties. In Proceedings of the Symposium on Friction Stir Welding and Processing, Indianapolis, IN, USA, 1 January 2001; pp. 15–23.
30. Zhang, X.; Xiao, B.L. A Transient Thermal Model for Friction Stir Weld. Part II: Effects of Weld A Transient Thermal Model for Friction Stir Weld. Part II: Effects of Weld Conditions. *Metall. Mater. Trans. A* **2011**, *42*, 3229–3239. [[CrossRef](#)]
31. Tufaro, L.N.; Manzoni, I.; Svoboda, H.G. Effect of Heat Input on AA5052 Friction Stir Welds Characteristics. *Procedia Mater. Sci.* **2015**, *8*, 914–923. [[CrossRef](#)]
32. Lammlein, D.H.; Gibson, B.T.; DeLapp, D.R.; Cox, C.; Strauss, A.M.; Cook, G.E. The friction stir welding of small-diameter pipe: An experimental and numerical proof of concept for automation and manufacturing. *Proc. Inst. Mech. Eng. Part B J. Eng. Manuf.* **2012**, *226*, 383–398. [[CrossRef](#)]
33. Thomas, W.M.; Nicholas, E.D.; Needham, J.C.; Temple-Smith, P.; Walter, S.; Kallee, K.W.; Dawes, C.J. Friction Stir Welding. UK Patent GB2306366A, 7 May 1997.
34. Colligan, K.J. Relationships between process variables related to heat generation in friction stir welding of aluminum. *Frict. Stir Weld. Process. IV* **2007**, *4*, 39–54.
35. Aissani, M.; Gachi, S.; Boubenider, F.; Benkedda, Y. Design and optimization of friction stir welding tool. *Mater. Manuf. Process.* **2010**, *25*, 1199–1205. [[CrossRef](#)]
36. Ebrahimzadeh, V.; Paidar, M.; Safarkhanian, M.A.; Ojo, O.O. Orbital friction stir lap welding of AA5456-H321/AA5456-O aluminum alloys under varied parameters. *Int. J. Adv. Manuf. Technol.* **2018**, *96*, 1237–1254. [[CrossRef](#)]
37. Aval, H.J.; Naghibi, M.F. Orbital friction stir lap welding in tubular parts of aluminium alloy AA5083. *Sci. Technol. Weld. Join.* **2017**, *22*, 562–572. [[CrossRef](#)]
38. Ismail, A.; Awang, M. Surface Hardness of Friction Stir Welded AA6063 Pipe. *MATEC Web Conf.* **2014**, *13*, 04025. [[CrossRef](#)]
39. Ismail, A.; Awang, M.; Rojan, M.A.; Samsudin, S.H. The characteristic of temperature curves for friction stir welding of aluminium alloy 6063-T6 pipe during tool plunging stage. *ARPN J. Eng. Appl. Sci.* **2016**, *11*, 277–280.
40. Chen, B.; Chen, K.; Hao, W.; Liang, Z.; Yao, J.; Zhang, L.; Shan, A. Friction stir welding of small-dimension Al3003 and pure Cu pipes. *J. Mater. Process. Technol.* **2015**, *223*, 48–57. [[CrossRef](#)]
41. Doos, Q.M.; Wahab, B.A. Experimental Study of Friction Stir Welding of 6061-T6 Aluminum Pipe. *Int. J. Mech. Eng. Robot. Res.* **2012**, *1*, 143–156.
42. D’Urso, G.; Longo, M.; Giardini, C. Microstructure and mechanical properties of Friction Stir Welded AA6060-T6 tubes. *Key Eng. Mater.* **2013**, *554–557*, 977–984. [[CrossRef](#)]
43. Gerçekcioglu, E.; Eren, T.; Yıldızlı, K.; Kahraman, N.; Salamci, E. The friction behaviour on the external surface of the friction stir welding of aa 6063- t6 tubes. In Proceedings of the Balkantrib’o5 5th International Conference on Tribology, Kragujevac, Serbia and Montenegro, 15–18 June 2005; pp. 225–228.
44. Yuan, S.; Hu, Z.; Wang, X. Evaluation of formability and material characteristics of aluminum alloy friction stir welded tube produced by a novel process. *Mater. Sci. Eng. A* **2012**, *543*, 210–216. [[CrossRef](#)]
45. Kumar, A.; Fairchild, D.P.; Macia, M.L.; Anderson, T.D.; Jin, H.W.; Ayer, R.; Ozekcin, A. Research progress on Friction Stir Welding of pipeline steels. *Proc. Bienn. Int. Pipeline Conf. IPC* **2010**, *2*, 711–719.
46. Khoureshid, A.M.; Sabry, I. Friction stir welding study on aluminum pipe. *Int. J. Mech. Eng. Robot. Res.* **2013**, *2*, 331–339.
47. Sabry, I.; El-kassas, A.M.; Khoureshid, A.M.; Hindawy, H.M. The joint properties for friction stir welding of Aluminum pipes. *IJAPIE* **2017**, *2*, 05–09.
48. Gopi, S.; Manonmani, K. Study of friction stir welding parameters in conventional milling machine for 6082-T6 aluminium alloy. *Aust. J. Mech. Eng.* **2012**, *10*, 129–140. [[CrossRef](#)]
49. Longhurst, W.R.; Strauss, A.M.; Cook, G.E.; Fleming, P.A. Torque control of friction stir welding for manufacturing and automation. *Int. J. Adv. Manuf. Technol.* **2010**, *51*, 905–913. [[CrossRef](#)]
50. Abdulstaar, M.A.; Al-Fadhalah, K.J.; Wagner, L. Microstructural variation through weld thickness and mechanical properties of peened friction stir welded 6061 aluminum alloy joints. *Mater. Charact.* **2017**, *126*, 64–73. [[CrossRef](#)]
51. Parashar, P.; Patel, A. A Review on Process Parameters on Tensile Strength and Hardness Testing of Friction Stir Welding Joint of Aluminium Alloys with Different Tool Pin Profile. *Int. J. Adv. Res. Ideas Innov. Technol.* **2018**, *4*, 277–281.
52. Okawal, Y.; Taniguichi, M.; Sugii, H.; Marutani, Y. *Development of 5-Axis Friction Stir Welding System*; IEEE: Piscataway, NJ, USA, 2006.
53. Soron, M.; Kalaykov, I. A robot prototype for friction stir welding. In Proceedings of the 2006 IEEE Conference on Robotics, Automation and Mechatronics, Bangkok, Thailand, 25–28 June 2006.
54. Mendes, N.; Neto, P.; Simão, M.A.; Loureiro, A.; Pires, J.N. A novel friction stir welding robotic platform: Welding polymeric materials. *Int. J. Adv. Manuf. Technol.* **2016**, *85*, 37–46. [[CrossRef](#)]
55. Smith, C. Robotic Friction Stir Welding using a Standard Industrial Robot. In Proceedings of the 2nd International Symposium on Friction Stir Welding, Gothenburg, Sweden, 27–29 June 2000; Volume 2.
56. Mendes, N.; Neto, P.; Loureiro, A.; Moreira, A.P. Machines and control systems for friction stir welding: A review. *Mater. Des.* **2016**, *90*, 256–265. [[CrossRef](#)]

57. Smith, C.B.; Crusan, W.; Hootman, J.R.; Hinrichs, J.F.; Heideman, R.J.; Noruk, J.S. Friction Stir Welding in the Automotive Industry. TMS Annual Meeting. Tower Automotive-Technology Application, 3533. 2001. Available online: https://www.researchgate.net/profile/Robert-Heideman/publication/268325940_FRICION_STIR_WELDING_IN_THE_AUTOMOTIVE_INDUSTRY/links/56092de308ae4d86bb1192a2/FRICION-STIR-WELDING-IN-THE-AUTOMOTIVE-INDUSTRY.pdf (accessed on 21 May 2023).
58. Ismail, A.; Awang, M.; Fawad, H.; Ahmad, K. Friction Stir Welding on Aluminum Alloy 6063 Pipe. In Proceedings of the 7th Asia Pacific IIW International Congress, Singapore, 8–10 July 2013; pp. 78–81.
59. Wang, G.; Zhao, Y.; Hao, Y. Friction stir welding of high-strength aerospace aluminum alloy and application in rocket tank manufacturing. *J. Mater. Sci. Technol.* **2018**, *34*, 73–91. [CrossRef]
60. Lotpy, M.A.M.N.; Ismail, A.; Rahman, F.A.; Zarina, M.K.P.; Baharudin, B.A.; Awang, M.; Hamid, D.A. Optimization of Welding Parameters for Self-Support Friction Stir Welding (SS- FSW) on AA6063 Pipe Joints. In *Advanced Engineering for Processes and Technologies II*; Advanced Structured Materials; Springer: Cham, Switzerland; Volume 147. [CrossRef]
61. Chowdhury, S.H.; Chen, D.L.; Bhole, S.D.; Cao, X.; Wanjara, P. Friction stir welded AZ31 magnesium alloy: Microstructure, texture, and tensile properties. *Metall. Mater. Trans. A Phys. Metall. Mater. Sci.* **2013**, *44*, 323–336. [CrossRef]
62. Vivek, C.M. A Review on Friction Stir Welding of Titanium Alloys. *Indian J. Sci. Res.* **2017**, *14*, 244–247.
63. Brassington, W.D.P.; Colegrove, P.A. Alternative friction stir welding technology for titanium–6Al–4V propellant tanks within the space industry. *Sci. Technol. Weld. Join.* **2017**, *22*, 300–318. [CrossRef]
64. Russell, M.J.; Blignault, C.; Horrex, N.L.; Wiesner, C.S. Recent Developments in the Friction Stir Welding of Titanium Alloys. *Weld. World* **2008**, *52*, 12–15. [CrossRef]
65. Ghosh, M.; Kumar, K.; Mishra, R. Analysis of microstructural evolution during friction stir welding of ultrahigh-strength steel. *Scr. Mater.* **2010**, *63*, 851–854. [CrossRef]
66. Lakshminarayanan, A.; Balasubramanian, V. Assessment of sensitization resistance of AISI 409M grade ferritic stainless steel joints using Modified Strauss test. *Mater. Des.* **2012**, *39*, 175–185. [CrossRef]
67. Emami, S.; Saeid, T.; Khosroshahi, R.A. Microstructural evolution of friction stir welded SAF 2205 duplex stainless steel. *J. Alloys Compd.* **2018**, *739*, 678–689. [CrossRef]
68. Wang, D.; Ni, D.R.; Xiao, B.L.; Ma, Z.Y.; Wang, W.; Yang, K. Microstructural evolution and mechanical properties of friction stir welded joint of Fe-Cr-Mn-Mo-N austenite stainless steel. *Mater. Des.* **2014**, *64*, 355–359. [CrossRef]
69. Kumar, S.S.; Murugan, N.; Ramachandran, K. Microstructure and mechanical properties of friction stir welded AISI 316L austenitic stainless steel joints. *J. Mater. Process. Technol.* **2018**, *254*, 79–90. [CrossRef]
70. Cui, H.; Xie, G.; Luo, Z.; Ma, J.; Wang, G.; Misra, R. Microstructural evolution and mechanical properties of the stir zone in friction stir processed AISI201 stainless steel. *Mater. Des.* **2016**, *106*, 463–475. [CrossRef]
71. Ismail, A.; Awang, M.; Rojan, M.A. An Effective Jig for Friction Stir Welding of Pipe Butt Joint. *Appl. Mech. Mater.* **2015**, 752–753, 491–495. [CrossRef]
72. Ismail, A. The preliminary experimental study of friction stir welding on aluminium alloy 6063 pipe butt joint. *Mar. Front. Mimetech. Bull.* **2013**, *4*, 1–7.
73. Ismail, A.; Awang, M.; Hamid, D.A.; Ab Rahman, F.; Khalid, P.Z.M. Temperature profile and fracture location of friction stir welded AA6063-T6 pipe butt joint. *ARPJ J. Eng. Appl. Sci.* **2016**, *11*, 13305–13308.
74. Steel, R.; Sterling, C.; Nelson, T.; Packer, S. Friction stir welding in pipeline applications. In Proceedings of the 2004 International Pipeline Conference, Calgary, AB, Canada, 4–8 October 2004; pp. 1515–1519. [CrossRef]
75. Vilaça, P.; Quintino, L.; Dos Santos, J.F. ISTIR—Analytical thermal model for friction stir welding. *J. Mater. Process. Technol.* **2005**, *169*, 452–465. [CrossRef]
76. Khan, N.Z.; Siddiquee, A.N.; Khan, Z.A.; Shihab, S.K. Investigations on tunneling and kissing bond defects in FSW joints for dissimilar aluminum alloys. *J. Alloys Compd.* **2015**, *648*, 360–367. [CrossRef]
77. Muthu, M.F.X.; Jayabalan, V. Tool travel speed effects on the microstructure of friction stir welded aluminum-copper joints. *J. Mater. Process. Technol.* **2015**, *217*, 105–113. [CrossRef]
78. Ganapathy, T.; Lenin, K.; Pannerselvam, K. Process Parameters Optimization of Friction Stir Welding in Aluminium Alloy 6063-T6 by Taguchi Method. *Appl. Mech. Mater.* **2017**, *867*, 97–104. [CrossRef]
79. Benavides, S.; Li, Y.; Murr, L.; Brown, D.; McClure, J. Low-temperature friction-stir welding of 2024 aluminum. *Scr. Mater.* **1999**, *41*, 809–815. [CrossRef]
80. Mishra, R.S.; De, P.S.; Kumar, N. Fundamental Physical Metallurgy Background for FSW/P. In *Friction Stir Welding and Processing*; Springer: Berlin/Heidelberg, Germany, 2014.
81. Gibson, B.T.; Lammlein, D.H.; Prater, T.J.; Longhurst, W.R.; Cox, C.D.; Ballun, M.C.; Dharmaraj, K.J.; Cook, G.E.; Strauss, A.M. Friction stir welding: Process, automation, and control. *J. Manuf. Process.* **2014**, *16*, 56–73. [CrossRef]
82. Kim, Y.; Fujii, H.; Tsumura, T.; Komazaki, T.; Nakata, K. Effect of welding parameters on microstructure in the stir zone of FSW joints of aluminum die casting alloy. *Mater. Lett.* **2006**, *60*, 3830–3837. [CrossRef]
83. Arbogast, W.J. A flow-partitioned deformation zone model for defect formation during friction stir welding. *Scr. Mater.* **2008**, *58*, 372–376. [CrossRef]
84. Dialami, N.; Cervera, M.; Chiumenti, M. European Journal of Mechanics/A Solids Defect formation and material flow in Friction Stir Welding. *Eur. J. Mech.-A/Solids* **2020**, *80*, 103912. [CrossRef]

85. Selvaraj, M. A temperature dependent slip factor based thermal model for friction stir welding of stainless steel. *Sadhana-Acad. Proc. Eng. Sci.* **2013**, *38*, 1393–1405. [[CrossRef](#)]
86. YSato, Y.S.; Urata, M.; Kokawa, H. Parameters controlling microstructure and hardness during friction-stir welding of precipitation-hardenable aluminum alloy 6063. *Met. Mater. Trans. A* **2002**, *33*, 625–635.
87. Silva, A.C.F.; De Backer, J.; Bolmsjö, G. Temperature measurements during friction stir welding. *Int. J. Adv. Manuf. Technol.* **2017**, *88*, 2899–2908. [[CrossRef](#)]
88. Khandkar, M.Z.H.; Khan, J.A.; Reynolds, A.P. Prediction of temperature distribution and thermal history during friction stir welding: Input torque based model. *Sci. Technol. Weld. Join.* **2003**, *8*, 165–174. [[CrossRef](#)]
89. Karthikeyan, L.; Kumar, V.S. Relationship between process parameters and mechanical properties of friction stir processed AA6063-T6 aluminum alloy. *Mater. Des.* **2011**, *32*, 3085–3091. [[CrossRef](#)]
90. D'urso, G.; Longo, M.; Giardini, C. Characterization of friction stir welded tubes by means of tube bulge test. *AIP Conf. Proc.* **2011**, *1353*, 1259–1264.
91. Aliha, M.; Ghoreishi, S.; Imani, D.; Fotoohi, Y.; Berto, F. Mechanical and fracture properties of aluminium cylinders manufactured by orbital friction stir welding. *Fatigue Fract. Eng. Mater. Struct.* **2020**, *43*, 1514–1528. [[CrossRef](#)]
92. Inácio, P.L.; Nogueira, F.; Ferreira, F.B.; Vidal, C.; Schell, N.; Tero, T.; Vilaça, P.; Oliveira, J.P.; Santos, T.G. Functionalized material production via multi-stack Upward Friction Stir Processing (UFSP). *Mater. Manuf. Process.* **2021**, *37*, 11–24. [[CrossRef](#)]
93. Mehta, K.P.; Vilaça, P. A review on friction stir-based channeling. *Crit. Rev. Solid State Mater. Sci.* **2021**, *47*, 1–45. [[CrossRef](#)]

Disclaimer/Publisher's Note: The statements, opinions and data contained in all publications are solely those of the individual author(s) and contributor(s) and not of MDPI and/or the editor(s). MDPI and/or the editor(s) disclaim responsibility for any injury to people or property resulting from any ideas, methods, instructions or products referred to in the content.